ACTIVE DEFORMATION OF THE SOUTH GRANITE MOUNTAIN FAULT SYSTEM: REACTIVATED COMPRESSIONAL FAULTS Vs. EXTENSIONAL OVERPRINTING

A Thesis

presented to

the Faculty of the Graduate School

at the University of Missouri-Columbia

In Partial Fulfillment

of the Requirements for the Degree

Master of Science

By

Michael R. Potter

Dr. Francisco Gomez, Thesis Supervisor

May 2022

The undersigned, appointed by the dean of the Graduate School, have examined the thesis entitled:

ACTIVE DEFORMATION OF THE SOUTH GRANITE MOUNTAIN FAULT SYSTEM: REACTIVATED COMPRESSIONAL FAULTS Vs. EXTENSIONAL OVERPRINTING

presented by Michael R. Potter,

a candidate for the degree of Master of Science,

and hereby certify that, in their opinion, it is worthy of acceptance.

Dr. Francisco Gomez

Dr. Brent Rosenblad

Dr. Eric Sandvol

ACKNOWLEDGEMENTS

I would first like to thank my research advisor, Paco Gomez, for his dedication and continued support throughout this project. Thanks to my committee members Eric Sandvol and Brent Rosenblad for their thorough feedback. Also, thanks Sean Polun for his help in planning the seismic survey and data collection and processing. Student field work assistants Spencer Anderson and Will Hunt worked hard and efficiently under difficult conditions, making this project feasible within a condensed time frame. I would like to thank my friends and family who have offered their love and support throughout this process. Thanks to the American Chemical Society's Petroleum Research Fund and the John & Betty Marshall Fund for Excellence (Department of Geological Sciences) for their monetary support. Finally, Thanks to the Department of Geological Sciences for their graduate student scholarship assistance.

TABLE OF CONTENTS

ACKNOWLEDGEMENTS ……...II

TABLE OF CONTENTS ……..III

LIST OF FIGURES ……..IV

ABSTRACT ……VI

CHAPTER 1: Introduction ……1

CHAPTER 2: Geologic Setting ……...11

2.1 Tectonic Evolution ……..11

2.2 Bedrock Geology…….14

2.3 Quaternary Geology ……15

2.4 Neotectonic Activity …….……..16

CHAPTER 3: Neotectonic Geomorphology ……28

3.1 Overview and Basic Idea ……28

Initial and Modified Scarp Conditions ……..……29

Degradation via the Diffusion Equation ……...……30

3.2 Data Acquisition: sUAV Photogrammetry ……..……31

sUAV Photogrammetry Data ……31

3.3 Scarp Profiling ……32

Scarp Profiling ……..……....32

Diffusivity Calibration ……..32

3.4 Results ……..……33

Single-Event Fault Scarp Profiles……..……33

Multi-Event Fault Scarp Profiles……...……34

CHAPTER 4: Shallow Geophysics ……..……47

4.1 Overview and Basic Idea ……47

4.2 Seismic Refraction……...……48

Data Processing ……..…49

4.3 Seismic Reflection ……...…50

Data Processing ……..50

4.4 Results …….……52

Rolling - Spread ……..……...……54

CHAPTER 5: Discussion and Conclusions…….…..……62

Implications for Seismic hazards …….…..…64

Future Work ……...……64

REFERENCES……...…66

LIST OF FIGURES

Figure 1.1 Tectonic map of the Western U.S ……5

Figure 1.2 Earthquake Focal Mechanism map of Laramide Region …….6

Figure 1.3 Physiographic map of Wyoming ……7

Figure 1.4 Schematic cross section of the Sweetwater Graben ……8

Figure 1.5 Active Fault map of Wyoming ……9

Figure 1.6 Photograph taken of fault scarp at Cherry Creek ……..……..10

Figure 2.1 Physiographic map of the Ferris Mountains ……19

Figure 2.2 Block models of Rocky Mountain uplifts ……...…20

Figure 2.3 Geomatrix Quaternary Surface site maps ……21

Figure 2.4 Geomatrix Paleoseismic Trench sketches ……24

Figure 2.5 Geomatrix extended cross section ……..…26

Figure 3.1 Fault Scarp Anatomy ……40

Figure 3.2 Digital Elevation Models ……...……41

Figure 3.3 Fault scarp profiles ……44

Figure 3.4 Structure from Motion aligned photos …….……45

Figure 3.5 Photograph of drone and pilot ……..……46

Figure 4.1 Fixed Spread seismic array ……..…….55

Figure 4.2 Seismic refraction tomography with raytracing ……...……56

Figure 4.3 Seismic refraction tomography with annotation ……..……57

Figure 4.4 Seismic reflection frequency filtered comparison ……58

Figure 4.5 Seismic reflection depth converted profile ……60

Figure 4.6 Seismic refraction and reflection profiles …….61

ACTIVE DEFORMATION OF THE SOUTH GRANITE MOUNTAIN FAULT SYSTEM: REACTIVATED COMPRESSIONAL FAULTS Vs. EXTENSIONAL OVERPRINTING

Michael R. Potter

Dr. Francisco Gomez Thesis supervisor

ABSTRACT

Quaternary faulting in and around Wyoming's Wind River Basin may pose a moderate earthquake risk for dams and other infrastructure within the region. The South Granite Mountains Fault Zone, located adjacent to the Wind River Basin, is one of several Quaternary faults in the region. The South Granite Mountains formed during the Late Cretaceous Laramide orogeny (75-45 Ma). Subsequently, during the Eocene, the extensive downfaulting and downfolding caused the Precambrian Mountain core to collapse forming the Sweetwater Graben. Recent Quaternary deformation is expressed as fault scarps along the north side of the Granite Mountains (2-4 meters). These features were originally studied in the 1980s but have received little attention since. In particular, the nature and style of faulting of this recent deformation was previously undocumented, and prior age estimates were broad. This study applies new methodologies to assess the active tectonics and earthquake potential of the South Granite Mountains Fault System. Low-altitude aerial surveying using drones facilitate the measurement and analysis of fault scarp morphology. From this scarp degradation modeling is applied to faulted surfaces with an age range of >201 to 16 ka. Results indicate long term dip slip rates between 0.01-0.05 mm/yr, and Horizontal extension rates between 0.01 – 0.03 mm/yr along the Ferris Mountains front. Shallow seismic reflection profiling is used to image

the fault geometry indicating normal faulting at high angles (83°). Offset of the unconformity between the Split Rock Formation and the Quaternary sediments is estimated at 10-13 meters. Using modern rates of faulting suggest quaternary faults initiated at 80-104 ka.

Chapter 1: Introduction

Active intraplate deformation in the Western U.S. is prevalent even in places that are often rarely considered. Quaternary faulting in the Wind River Basin (south central Wyoming) remains enigmatic and poorly understood to this day. The Wind River Basin occupies over 22,014 square kilometers of central Wyoming and is typical of the large structural and sedimentary basins that formed during the Laramide deformation in the Rocky Mountains region (***Figure 1.1 and 1.2***). It is bounded by the southern Bighorn mountains, Owl Creek, and Washakie ranges to the north, Wind River range to the west, the Casper arch to the east, and to the south by the Granite Mountains (***Figure 1.3***). Within this context, the South Granite Mountain Fault System (SGMFS) spans 135 kilometers along the southern margin bounded by the Ferris, Green, and Seminoe mountains to the south and the down dropped Sweetwater graben to the north (***Figure 1.4***). The SGMFS has previously been studied along the Ferris and Green Mountains segments with neotectonic focus on slip rate constraints (Geomatrix Consultants, 1988). This work, however, focuses exclusively on the Ferris mountains segment, an area that may display reactivation of Laramide faults. Using landscape elements (i.e., scarp morphology and fault geometry), the Ferris Mountains segment of the SGMFS is a key location for assessing the role of fault reactivation on Cenozoic intraplate tectonics.

Quaternary tectonism has produced faults scarps which can be used as geologic markers for quantifying recent deformation across the Wind River Basin (***Figure 1.5***). The Ferris Mountains segment contains fault scarps that cut through quaternary geomorphic benches producing vertical offsets between 2-4 meters (as seen at Cherry Creek). These scarps are evidence for pre-historic surface rupturing earthquakes through

morphological analysis. The purpose of this project is to assess the geometric relations and kinematics of faulting along the Ferris Mountains segment of the SGMFS (i.e., fault dip and deformation rate), the history and recurrence of fault displacement (i.e., earthquake magnitudes and recurrence intervals), and the migratory patterns of seismic and tectonic activity (i.e., progression or regression of earthquake activity and deformation rates). In addition, comprehensive analysis of deformation rates and earthquake activity is achieved through correlation to surrounding fault segments.

Past works have generally assumed that the scarps associated with the SGMFS are normal faults (Love, 1970). However, faults of a similar character observed in the northern part of the basin along the Owl Creek Mountains display reactivation of older reverse oriented Laramide faults (Gomez et. al, 2016). I propose two hypotheses for the geometry and style of faulting within the SGMFS:

1. High angle normal faulting (>60 degrees north) associated with gravitational collapse of the Granite Mountains core resulting in basin-ward dips. Faulting in this case would represent the continued extensional collapse of the Granite mountains and the Sweetwater Graben.
2. Reactivation of older Laramide high angle (>60 degrees) reverse faults resulting in mountain-ward dips. Deformation in this case would represent a change in the local stress regime.

Analysis addressing the nature of the SGMFZ to provide a basis for testing model predictions is achieved through two modes:

1. Scarp degradation analysis is conducted utilizing localized, detailed micro-geomorphologic features to assess the active rates of slip along the fault plane.

The geomorphic characteristics of young fault scarps ban be useful in evaluating the probable ages of fault displacement. Additionally, without radiometric dates, alternative methods need to be employed for quantitative assessments. Therefore, fault-scarp analysis through degradation modeling allows for the assessment of the scarp's age and uplift rate. Magnitude constraints on paleo-earthquakes can be inferred from the scarp height (Hanks et al., 1984; Wells and Coppersmith, 1994). A ranking of these fault scarps according to their relative geomorphic ages can be conducted based on these age estimates and applied to a general framework between several hundred to several thousand years old.

2. Shallow seismic imaging is applied to constrain fault geometry which will correlate to the surface kinematic results. The location of the seismic line was chosen based on what was deemed a viable fault scarp (i.e., observable in aerial imagery). Seismic refraction and reflection methods were used and combined, these data attempt to comprehensively assess the fault's location, and geometry.

By these means this project attempts to quantify the characteristics of scarp morphology (photogrammetric methods) and model the underlying structures (subsurface geophysical methods), in order to test proposed hypotheses on the style and rates of faulting

In addition to the implications for diffuse, continental deformation, the results of this study also contribute to the improving the earthquake hazard assessment in the Wind River Basin. In addition to naturally occurring seismicity, the potential for triggered earthquakes resulting from ongoing hydrocarbon extraction and waste fluid injection is

possible. To protect the existing infrastructure from the risk damage by earthquakes, the accurate characterization of the region's seismicity is needed.

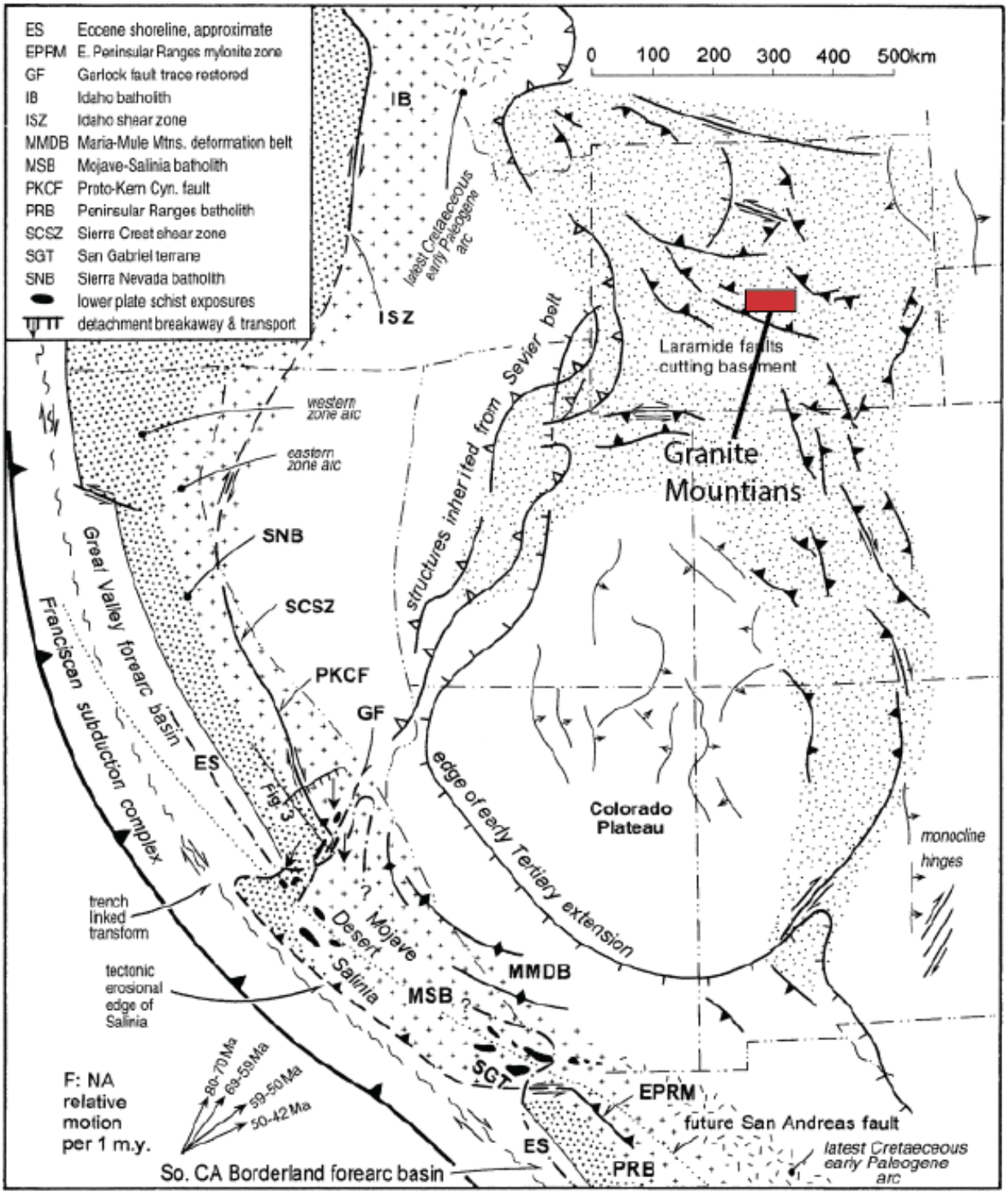

Figure 1.1 – Tectonic map of the Western us adapted from Saleeby (2003).

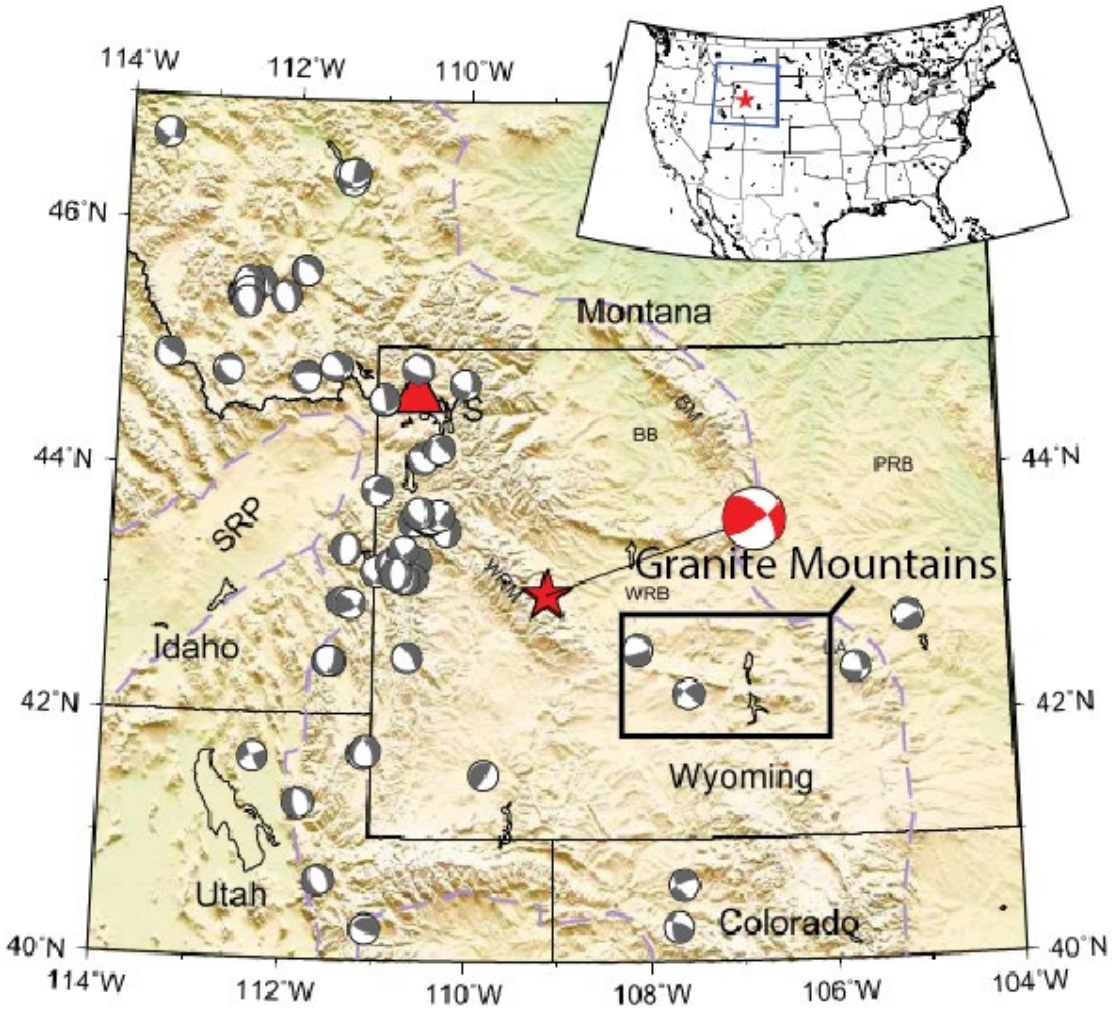

Figure 1.2 – Earthquake focal mechanism map of Wyoming and other nearby locations. The red focal mechanism on this map is a mantle source earthquake, the gray focal mechanisms are all crustal sourced earthquakes. Two focal mechanisms appear in the Granite Mountains region, a normal fault to the west and a strike slip fault further east from Wang et al. (2016).

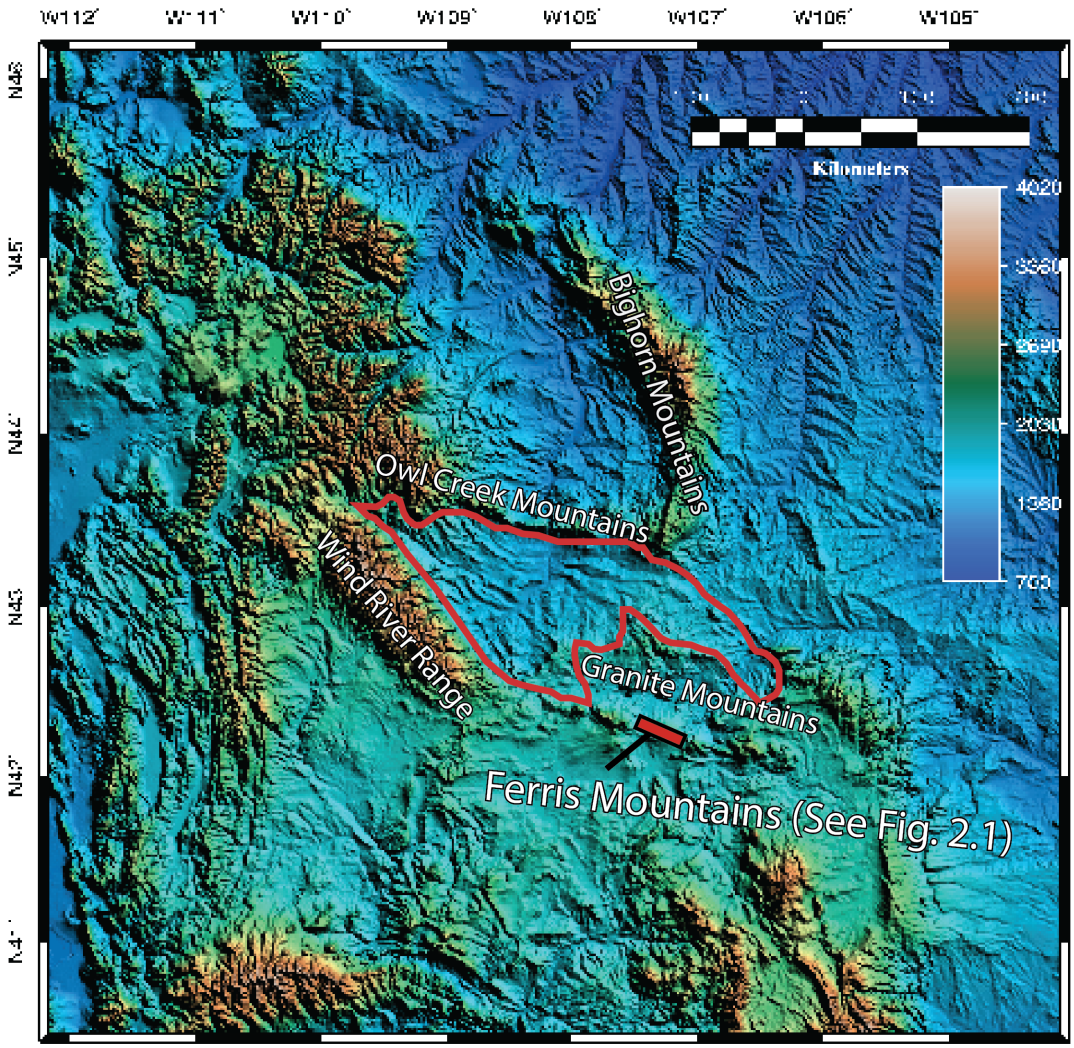

Figure 1.3 **–** Physiography of Wyoming, showing the location of the Wind River Basin and surrounding mountain ranges. For Ferris Mountains physiography see figure 2.1.

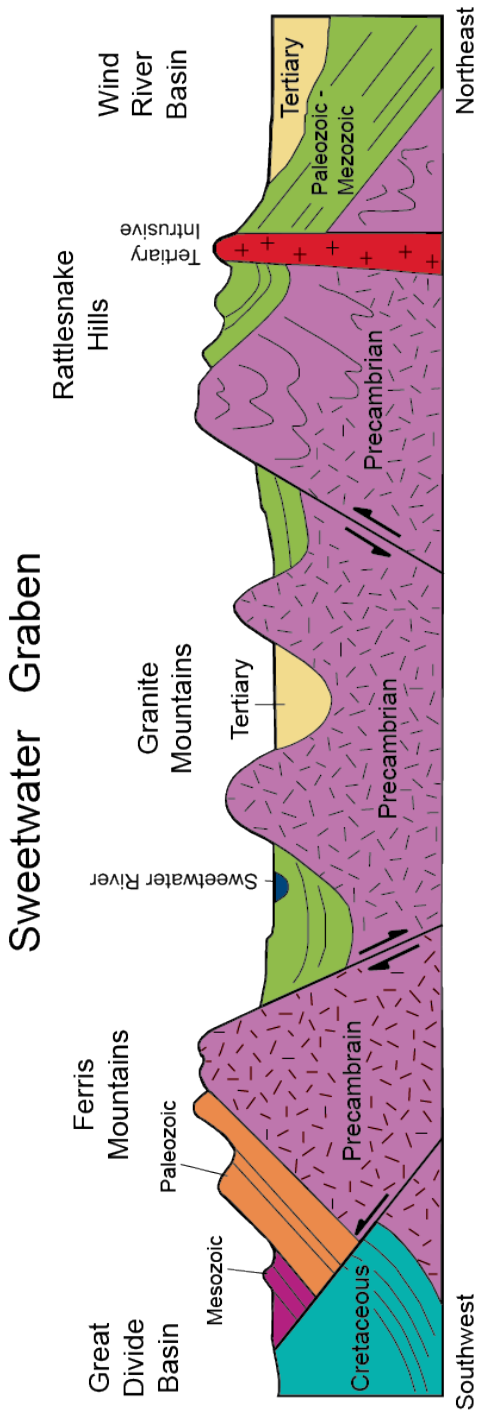

Figure 1.4 – Schematic cross section of the Sweetwater Graben (not to scale) adapted from Mears et al. (1986).

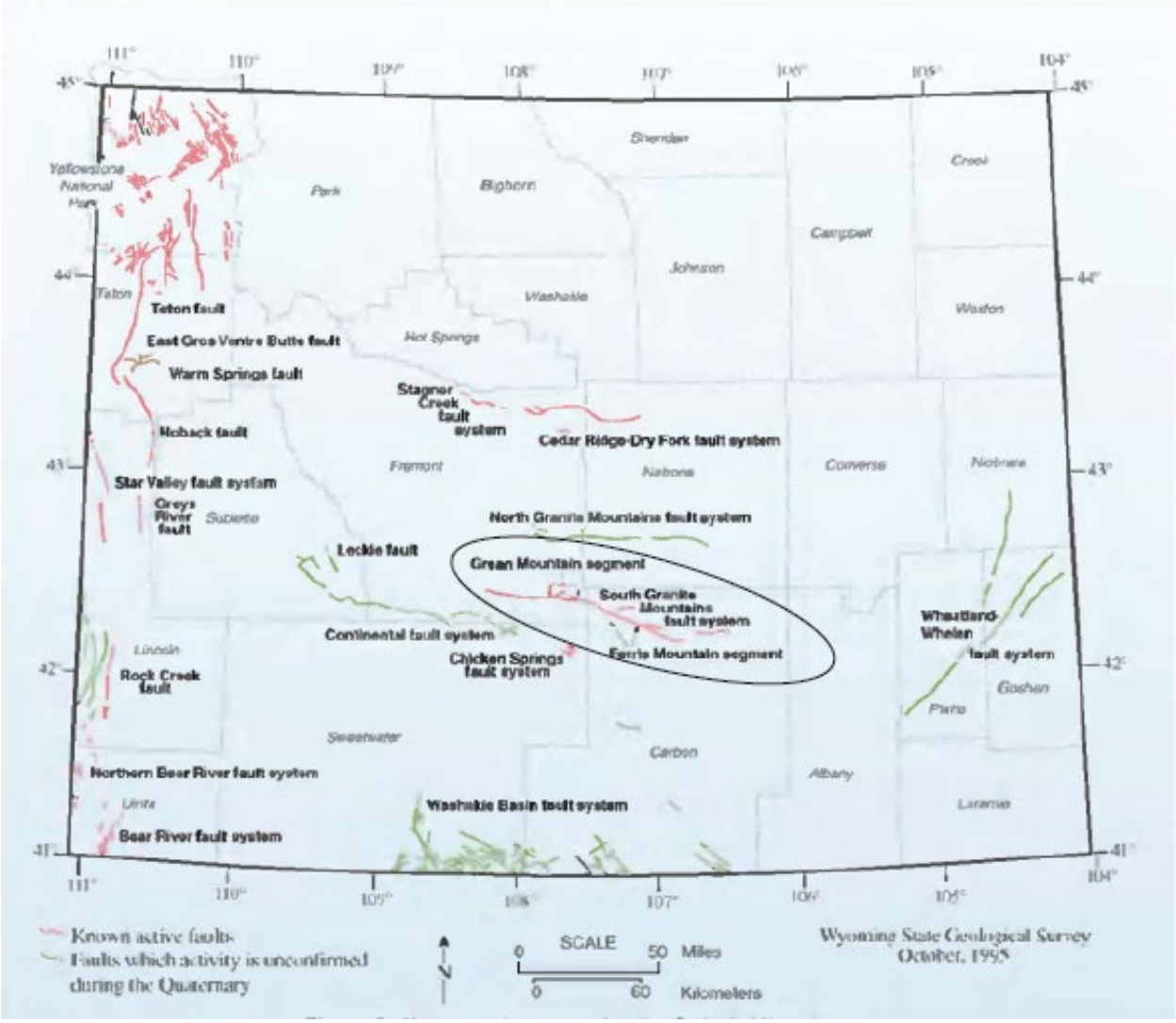

Figure 1.5 – Active fault map of Wyoming denoting the location of the SGMFS, adapted from Case and Green (2000).

Figure 1.6 – Field photograph of the scarp at Cherry Creek taken facing southward toward the Ferris Mountains interior. Scarp height is approximately 2 meters

Chapter 2: Geologic Setting

2.1 Tectonic Evolution

Wyoming's Wind River Basin is situated in central Wyoming and bounded by several mountain ranges of 3 of its sides including the Wind River, Owl Creek, Bighorn, and Granite Mountains (***Figure 1.1***). The Granite Mountains block bounds the southern margin of the basin and is a large structurally down dropped block often times referred to in the literature as the Sweetwater Graben or Sweetwater Uplift (Blackstone, 1991), named for the river that flows through the region. On either side of the down dropped block are raised topographic regions, to the north these are the Rattlesnake Hills, and to the south are the Seminoe, Ferris (***Figure 2.1***), and Green Mountains. The Granite Mountains were uplifted and eroded during Laramide deformation. Extensive down-warping and down-folding in post – early Eocene time led to collapse pf the Precambrian core which was then subsequently buried by tertiary sediments (Keefer, 1970). The SGMFS is the boundary that separates the southern mountain ranges from the graben block. The origins of this fault system and the style of deformation along it are the subject of inquiry and are explored in depth in this study.

The structural style characteristic of the Rocky Mountain foreland is that of Precambrian crystalline basement cored uplifts separated by deep basins termed "thick-skinned" deformation (Snoke, 1993). The Wind River Basin (located in this region) displays a wide variation in structural trends with mountain ranges oriented in nearly every compass direction (Allmendinger, 1992). It has been postulated that the orientations of these basement uplifts are controlled in part by the paleotectonic events in the region, and there are strong correlations elsewhere in the Rocky Mountains province,

but the Archean basement rocks beneath Wyoming and the Wind River Basin were left relatively unaffected by the Ancestral Rocky Mountains event and more closely coincides with the with the edge of the Precambrian Belt Basin of Montana. Reactivation of these older structural trends though have only been demonstrated in a few locations as the structures of the Rocky Mountain foreland crosscut the older trends (Allmendinger, 1992). Industry seismic data indicates shortening of the Rocky Mountains foreland underwent horizontal shortening along moderate to high angle (30-90 degrees) reverse faults (***Figure 2.2***). Normal faulting is then associated with younger Cenozoic extension where these faults are generally confined to the hanging wall blocks of the uplifted blocks causing the collapse of the upper plate. This geometry is noted by Allmendinger (1992) as being particularly obvious in the Granite Mountains. Blackstone (1991) makes the claim that additional data derived from mapping, drilling, and industry seismic reveals these faults dip in the same direction as the reverse faults they are associated with and are best interpreted as listric normal faults.

The Granite Mountains structural development consists of eight phases as listed by Love (1970). The first phase of structural evolution began with gradual vertical uplift of the mountain arch, coinciding with subsidence of Wind River and Great Divide basins to the north and south during the late Cretaceous. The second phase displayed an increase in the magnitude of vertical uplift of the mountain arch and decrease in amount of subsidence of flanking basins. The third phase of development saw uplift of the Granite Mountains predominated over subsidence of flanking basins and the development of subsidiary folds trending northwest. Also, the development of thrust faults along steep flanks of the mountains and subsidiary anticlines form during the early Eocene. The

compressive force resulting in this uplift would have been oriented with a southwest trend. Phase four saw vertical uplift of the west-trending, central part of the Granite Mountains and the anticlinal-synclinal complex to the west along normal faults during the transition from early to middle Eocene. The mountains and basins remained stable for 20 million years marking the fifth phase of development. The sixth phase of developments starts in the Miocene with the Granite Mountains arch and anticlinal-synclinal complex to the west subsiding as a single unit. The Split Rock syncline developed as the new dominant structural feature along its east trend across both the complex and the highest part of the Granite Mountains. Epeirogenic uplift of the region occurred simultaneously with downfaulting of the Granite Mountains core during the Pliocene, marking the seventh phase of development. Faulted areas to the west reactivated the North and South Granite Mountains fault systems reversed in the direction of displacement as the Split Rock syncline continued to subside. Much of the post Eocene strata deposited in the Great Divide Basin was then stripped away with the debris then being dumped on the foundering Granite Mountains. The final phase of development displayed the continued sinking of the Split Rock syncline and the development of a broad east-trending arch in the southern Wind River Basin during the Pleistocene. Antecedent drainage across the Seminoe Mountains, and superposition the drainage systems were established at this time. Erosion across the Wyoming resulting from the Epeirogenic uplift was vigorous, yet the continued subsidence of the Granite Mountains resulted in the remarkably complete Cenozoic depositional and tectonic history being preserved (Love, 1970).

2.2 Bedrock Geology

The Granite Mountains are distinctive from the other mountain ranges in Wyoming for the fact that they remain partially buried by Cenozoic strata. This preservation of materials was made possible by the subsidence of the mountain range during the Cenozoic prior to or contemporaneously with an epeirogeny uplift that would have initiated the current degradation cycle. The Granite Mountains core is composed of Precambrian metamorphic and granitic rocks. The granite is considered to be part of a batholith whose age of emplacement is between 2,450 and 2,650 million years ago. Diabase dikes and sills as well as older mafic dikes crosscut the plutonic rocks, however the ages obtained from the diabase are interpreted to be erroneous by Peterman and Hildreth (1978). These Precambrian rocks would have undergone alteration as part of a thermal episode sometime later which resulted in disturbed mineral ages obtained through Rb-Sr and K-Ar methods (Peterman and Hildreth, 1978).

The Precambrian Granite Mountains core is overlain by a series of Paleozoic and Mesozoic sedimentary strata that predate the Eocene collapse. Truncating these older strata are the younger Cenozoic sediments that were deposited on a surface of low to high relief, which make up the flanks of the mountain core (Love, 1970). This overlapping of strata is complicated by a variety of processes including large scale faulting, reversal of direction of motion on high angle faults, etc. and has led to a complex history of sedimentation. In general, these strata are sediments deposited on the stable marine shelf on the eastern side of the North American Cordilleran (Keefer, 1965). Little more attention is paid to the overlapping strata, but it is noted that it is source material for the

younger Tertiary and Quaternary units that fill the graben basins and truncate the Precambrian basement material along the SGMFS.

The Tertiary units that makeup the strata infilling the Wind River Basin have been detailed in depth by Love (1970) for their distributions, lithologies, stratigraphy and structural relations. The more general progression of deposition can be described as lacustrine deposits on the mountain flanks from locally derived sediments during the Paleocene. During continued basin subsidence the central portion of the basin was flooded then by Waltman Lake. Early Eocene clastic accumulation in alluvial fans along the highlands surrounding the basin. Also continued fine grained sedimentation towards the basin interior. Sediment would have been locally derived as the highlands around the basin continued to erode. Towards the end of the early Eocene, volcanic materials supplied form the Absaroka-Yellowstone region were deposited. Throughout the middle and late Tertiary sedimentation can be described as nearly continuous aggradation. From the Oligocene to the Pliocene volcanic sediments were supplied and produced a sharp contrast to the earlier clastic deposition. Then uplift of the basin in the late Pliocene set off the degradation cycle which has excavated away much of these units and left the units of the lower Eocene and older current observation (Keefer, 1965).

2.3 Quaternary Geology

The Quaternary deposition in the Granite mountains region of Pleistocene and younger material is described by Love (1970). This includes deposits of airfall ash and locally sourced alluvial sediments. In the area of the SGMFS along the Ferris mountains segment, the ashfall sediments are not observed. The locally derived sediments in the region present sands and clay along the Sweetwater River valley, pediment gravels, and

sand held in both stabilized and active dunes. The inclined upland surfaces along the Ferris, Green, and Crooks Mountains segments are capped by gravels that reflect a complex depositional history due to motion along the fault system. They can generally be described as debris of coarse sand, gravels, and boulders. These Quaternary surfaces have been offset in several locations along the SGMFS and are described by Jaworowski (1988) and Geomatrix Consultants inc. (1988) report.

2.4 Neotectonic Activity

Neotectonic activity has been observed offsetting the Quaternary surfaces along several segments of the SGMFS. These surfaces were the subject of work done by Geomatrix Consultants inc. (1988) and Jaworowski (1988). The faulted surfaces of focused on by Jaworowski, 1988 are found in the Green Mountains segment. Three surfaces are noted as being offset here with those being the Willow Creek bench (100,000 yrs B.P.), the Telephone Line Ridge bench (300,000 yrs B.P.), and the pre-Telephone Line Ridge bench (600,000 yrs. B.P.) with and average scarp height of 8m, indicates the SGMFS along the Green Mountains segment has likely seen several episodes of faulting since 600,000 yrs. B.P. but no tighter age constraint is offered.

The Geomatrix Consultants inc., report focuses on several Quaternary faults within the Wind River Basin, with respect to the SGMFS the Seminoe, Ferris, Green, and Crooks Mountains, and the Muddy Gap Segments are all described in detail. The faults scarps here are described as dip-slip down-on-the-north, but the fault block geometry is not identified as faults are made vertical. Along the Ferris Mountain segment, sight investigations were done at East Arkansas, Pete, and Cherry Creeks (***Figure 2.3***). At the Cherry Creek location paleoseismic trenches were also excavated (***Figure 2.4-2.5***). From

Arkansas to Pete Creek the fault is a nearly linear, continuous segment that crosses all but the youngest surface. The surfaces being cut are of at least 3 different ages respectively. A numerical estimate of the ages of the surfaces at Arkansas and Pete creek was not completed due to the lack of soil data and dating material, but it is inferred that they formed between the middle Pleistocene to Holocene. At the Cherry Creek site, the fault is also nearly continuous and displaces several Quaternary surfaces. The surface Q4c lies across the Fault Trace and is not offset, thus it is used to constrain the age of the most recent displacement. This surface is dated to be between 2,000 and 7,000 yrs. B.P. based on its soil characteristics making the most recent displacement at this location happening before this surface formed. The surfaces that have been displaced in this location are considered to be post-Bull Lake to Pinedale age (15,000 to 190,000 yrs B.P.) placing a wide initial age estimation for displacement along this portion of the fault descriptions of these surfaces appear in ***Table 2.1***.

The Ferris and Green Mountains segments of the SGMFS are the only known active faults close enough to any critical infrastructure (dams in the case of the Geomatrix report) to produce significant ground shaking to cause seismic hazards. It is estimated that for both of these segments the possible range for earthquake magnitudes would fall between magnitudes 6.4 to 6.9 with a preferred estimate of 6.6. This estimate is contingent on a rupture along the entire length of fault segment (17-23 km) and a rupture area of 306 – 414 square km for the Ferris Mountains, and 408 – 522 square km for the Green Mountains segments respectively. This would generate an estimated displacement of 0.6m (Geomatrix Consultants inc., 1988). Estimated recurrence along the Ferris mountains segment is wide depending on the estimated magnitude and can range from

>5,100 years to 16,000 years. Similarly for the Green Mountains segment the estimated recurrence interval is to be between 4,500 and 12,000 years per event. The wide range of calculated recurrence intervals reflects a high degree of uncertainty for a fault that data indicates exhibits a low degree of activity. This suggests that the recurrence interval for the fault is at least several thousand years and may be longer than 10,000 years (Geomatrix Consultants inc., 1988).

.

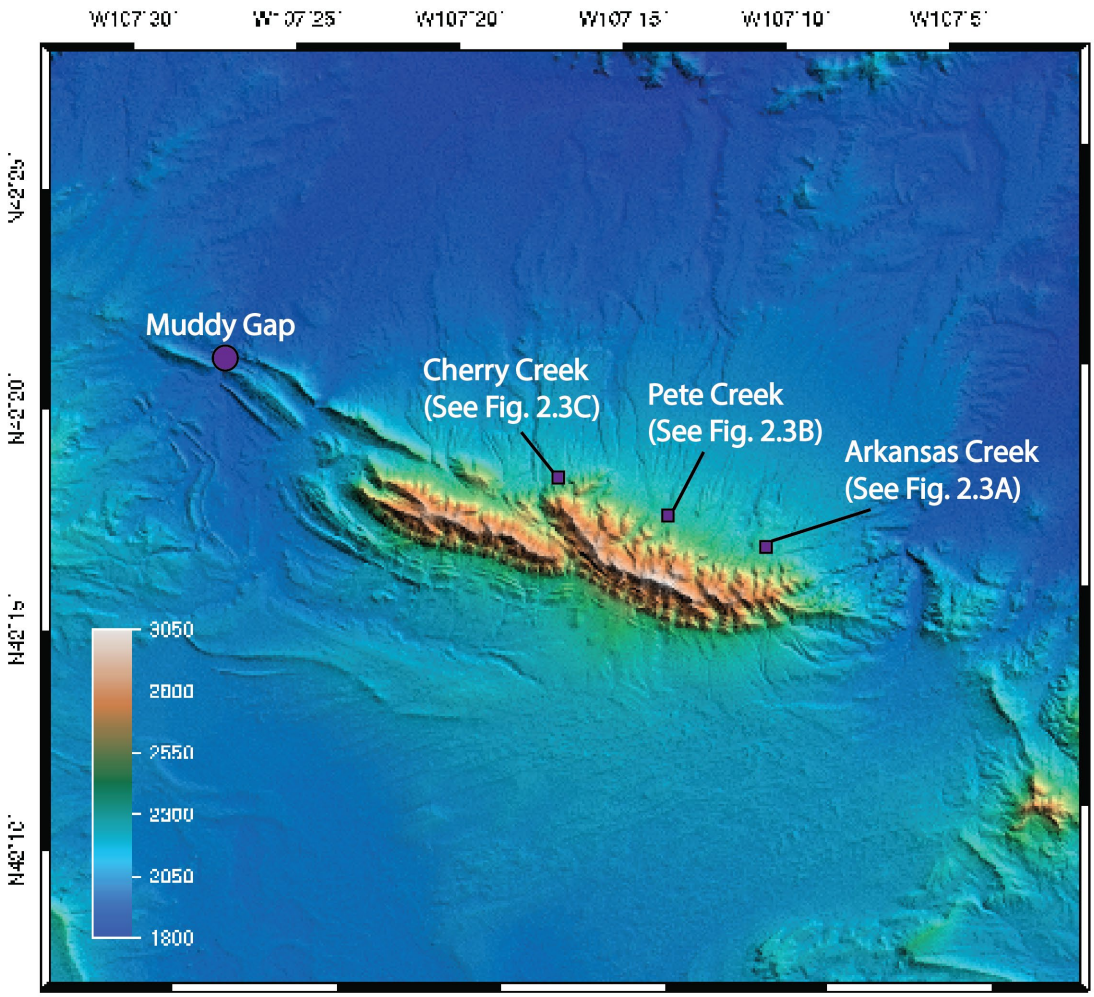

Figure 2.1 – Physiographic map of the Ferris Mountains segment of the Granite Mountains denoting site investigation locations.

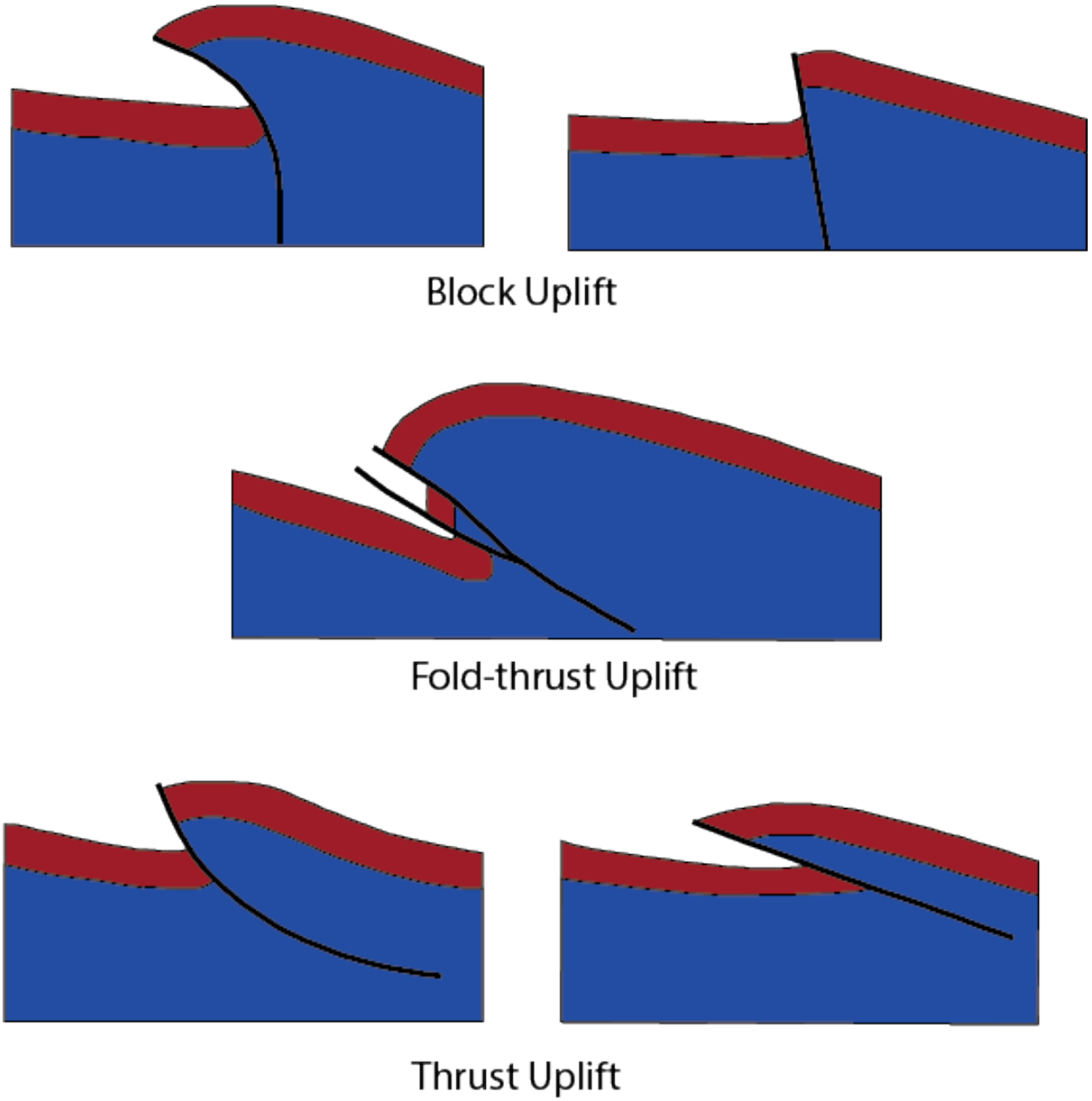

Figure 2.2 – Block models of reverse faulting for the Rocky Mountains foreland adapted from Allmendinger (1992).

A

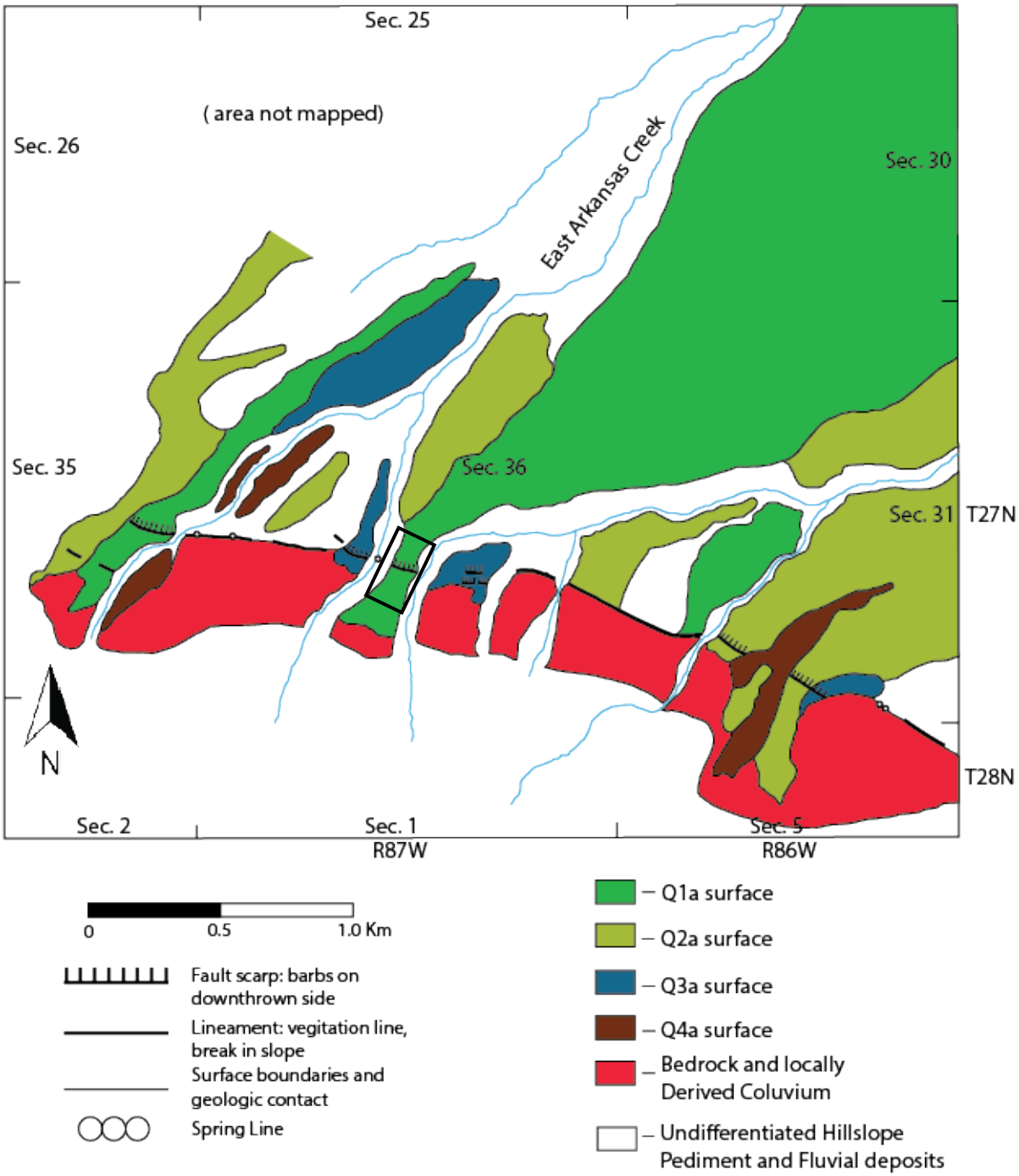

Figure 2.3A - Site sketch maps of quaternary surfaces (adapted from Geomatrix consultants inc., 1988) at Arkansas Creek field location. Boxes show approximate photogrammetry survey extents.

B

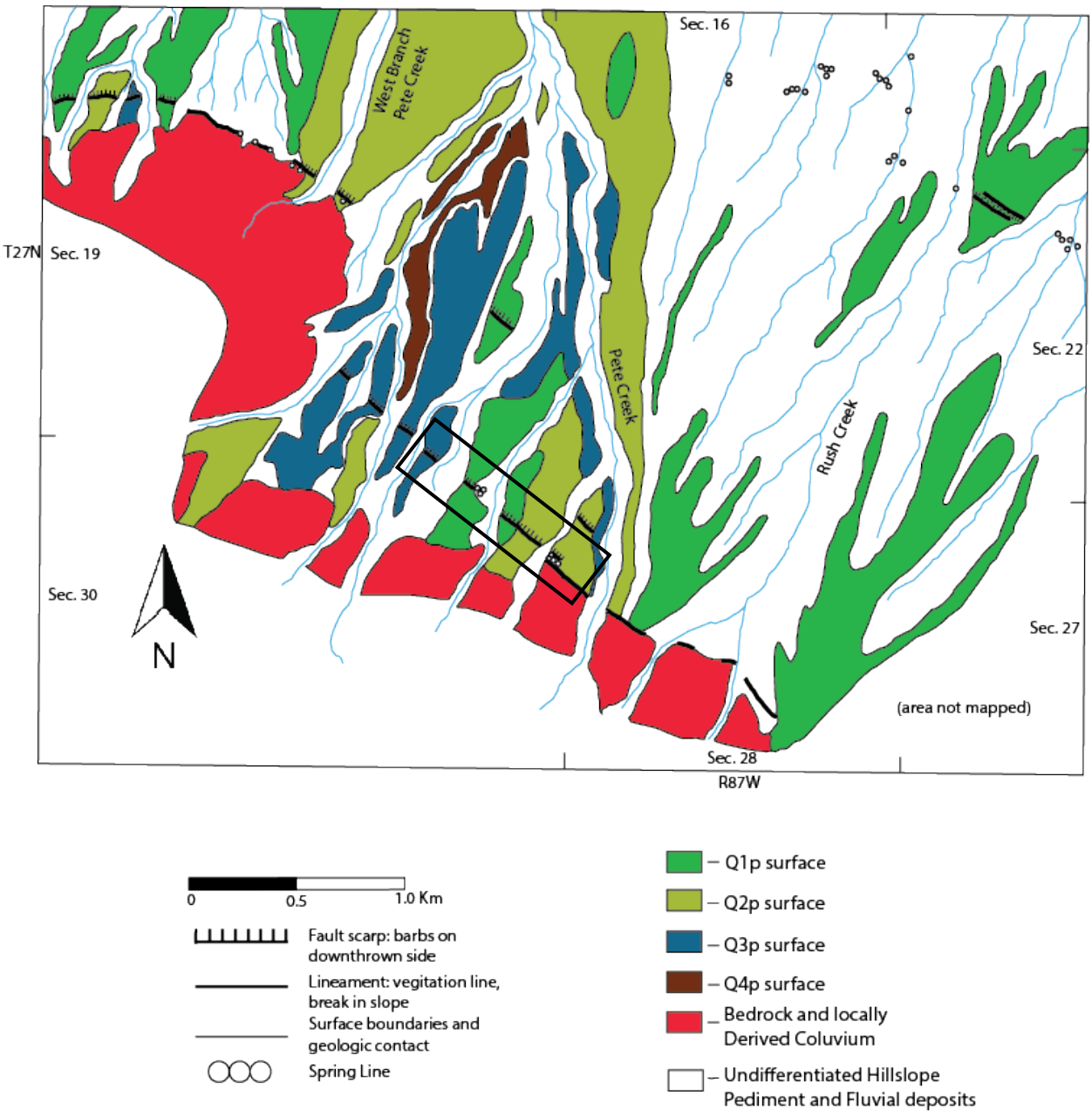

Figure 2.3A - Site sketch maps of quaternary surfaces (adapted from Geomatrix consultants inc., 1988) at Pete Creek field location. Boxes show approximate photogrammetry survey extents.

C

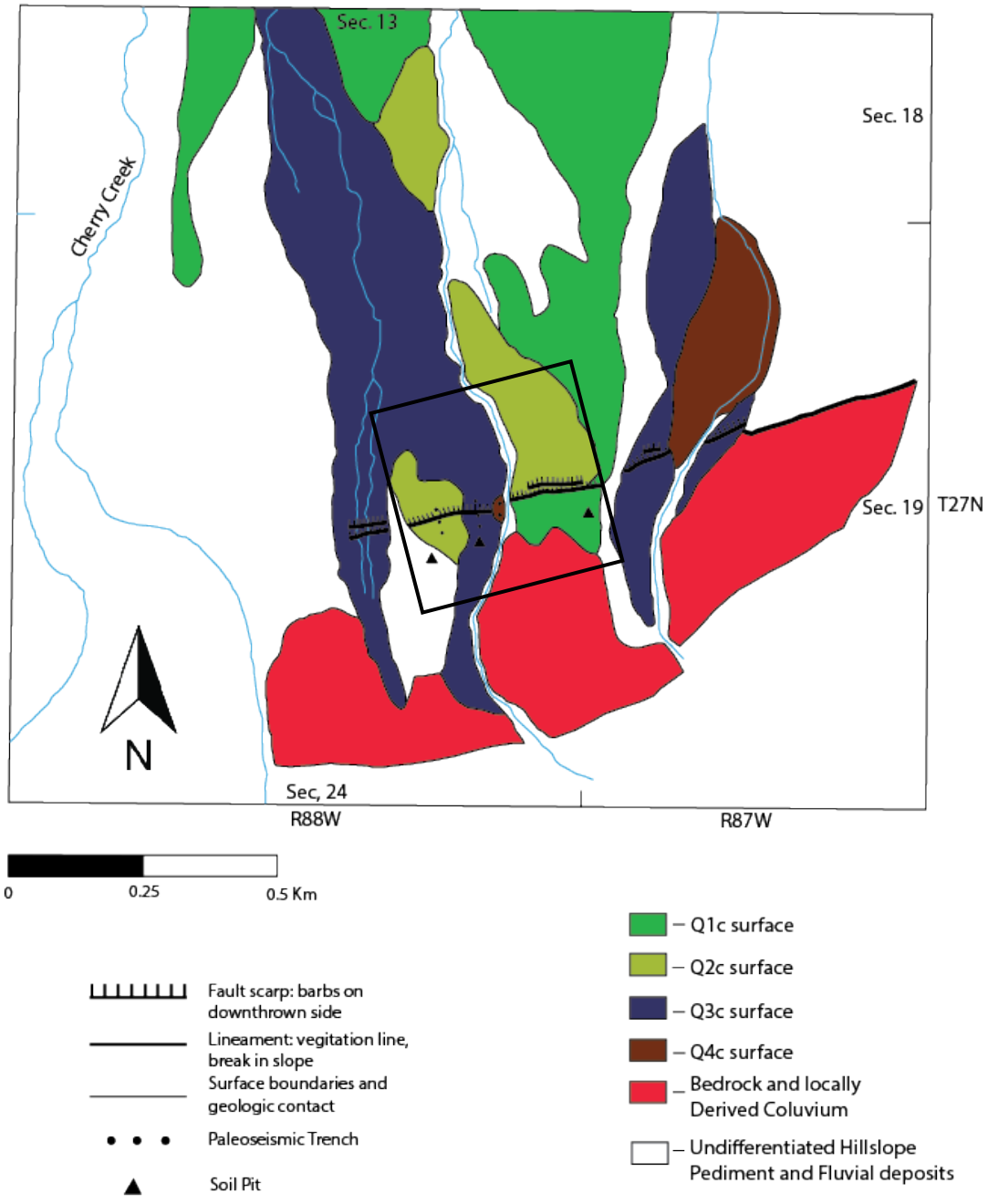

Figure 2.3C – Site sketch maps of quaternary surfaces (adapted from Geomatrix consultants inc., 1988), at Cherry Creek field location. Boxes show approximate photogrammetry survey extents.

A

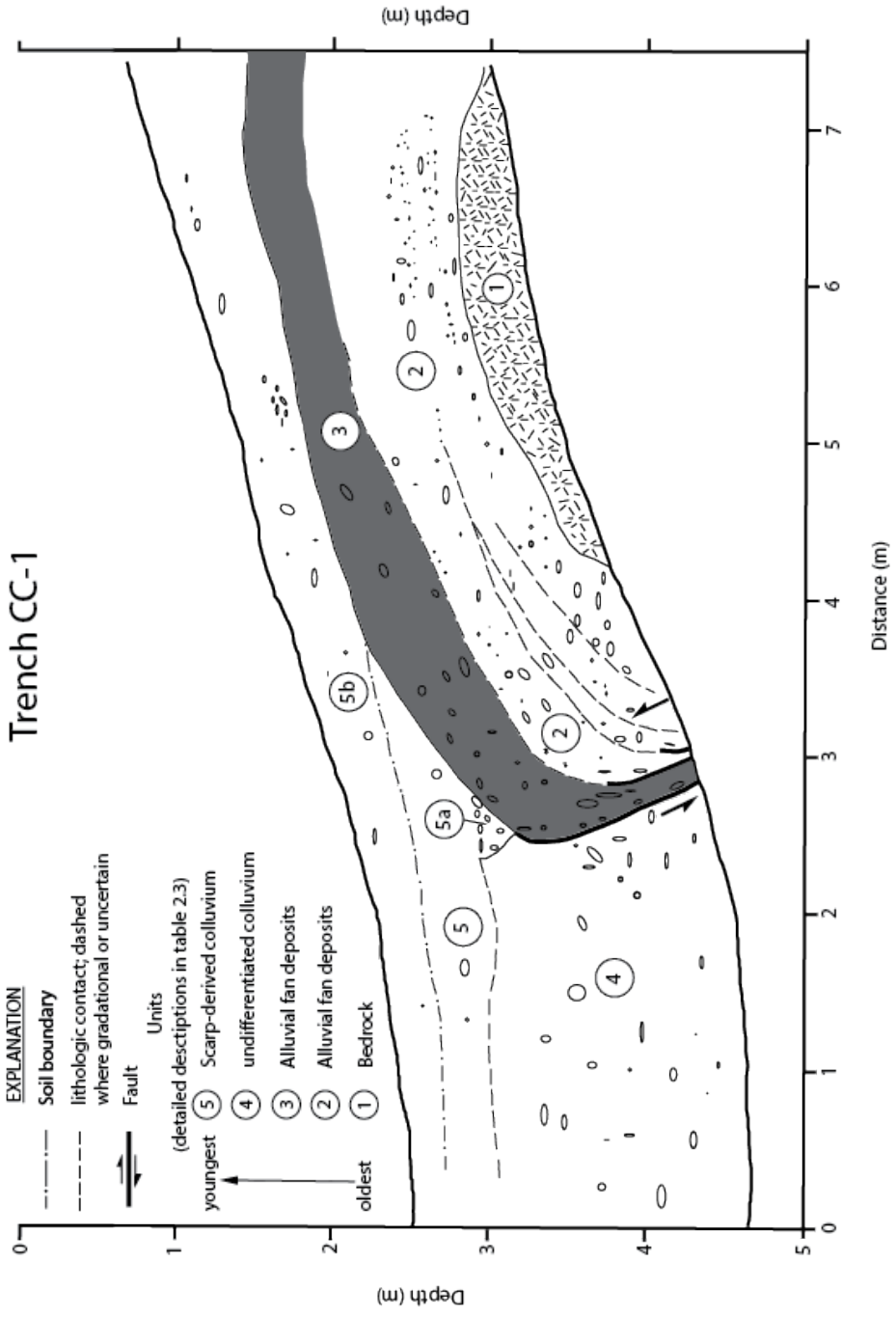

Figure 2.4A – paleoseismic trench sketches from the Cherry Creek location trench CC-1 showing potential reverse faulting (from Geomatrix Consultants inc. 1988).

B

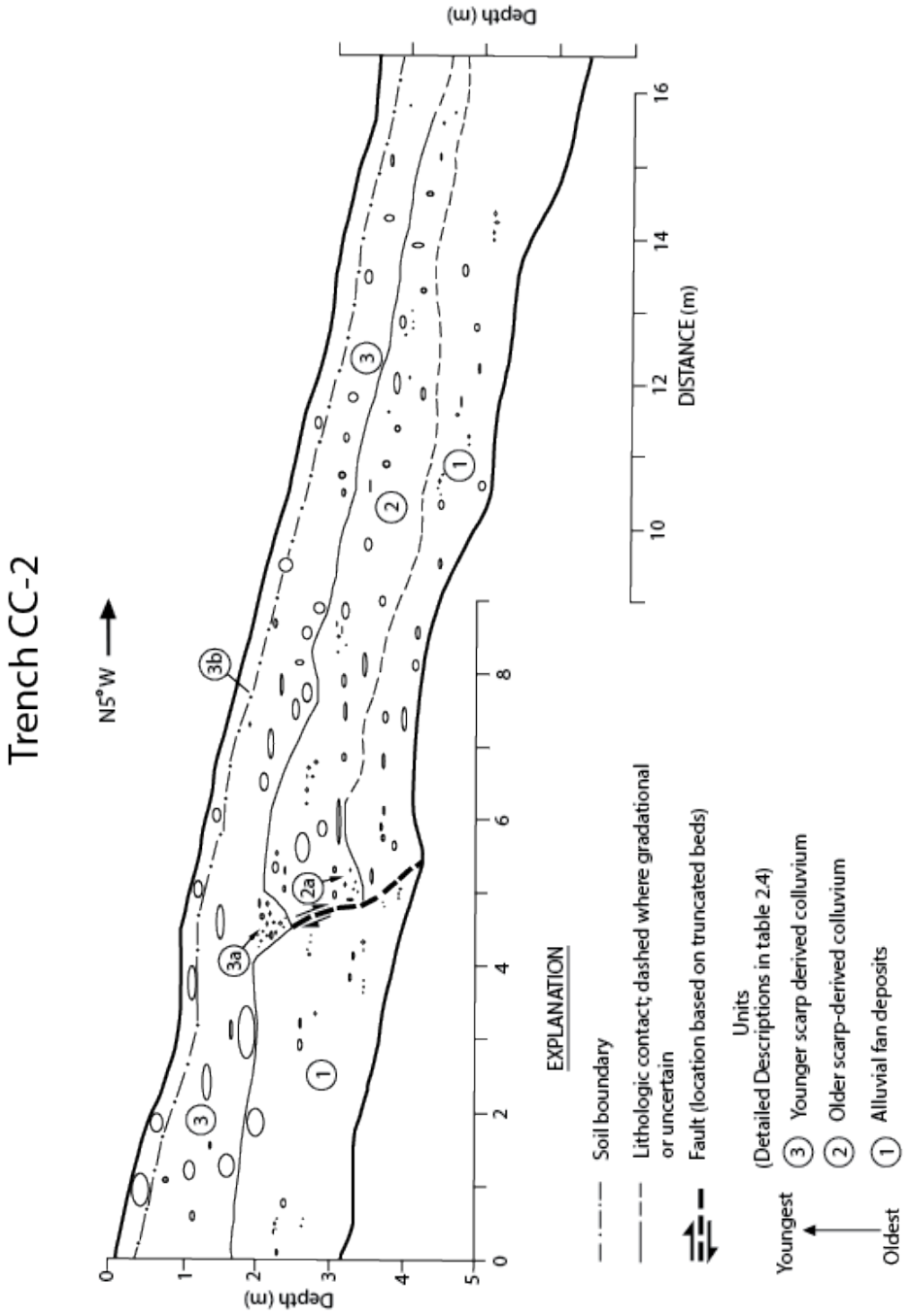

Figure 2.4B – paleoseismic trench sketches from the Cherry Creek location trench CC-2 showing normal faulting (from Geomatrix Consultants inc. 1988).

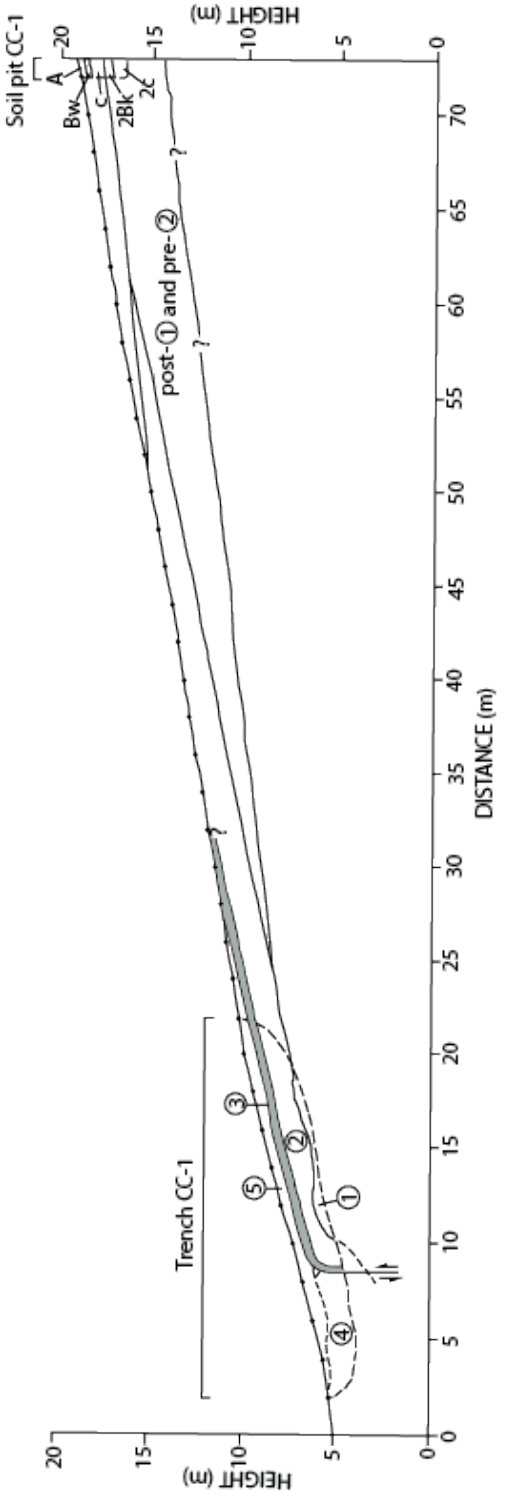

Figure 2.5 – Cross section extended from trench cc-1 upslope to soil pit cc-1 at Cherry Creek, here the fault is made vertical (Geomatrix Consultants inc., 1988)

Table 2.1 Surface and Soil Characteristics (Geomatrix Consultants inc., 1988)

Geomorphic Surface	Slope	Surface Displacement	Soil Hue
Q1c	8-10 degrees	4.3 + / - 0.2m	7.5 YR
Q2c	9 degrees	1.4 + / - 0.1m	10 YR
Q3c	13 degrees	1.0 + / - 0.1m	10 YR
Q4c	NA	0m	NA

Chapter 3: Neotectonic Geomorphology

3.1 Overview and Basic Idea

To address the neotectonic nature and kinematic evolution of the SGMFS several steps were applied to measure, characterize, and analyze the fault scarps morphology. In every surface material (e.g., bedrock, unlithified sediment), fault scarp morphology changes over time; the degree and rate in which this these changes occur are pertinent when assessing the local seismic hazard. The two main factors contributing to the rate of fault-scarp morphology are weathering and transport; the slopes change reflects the more dominant process (i.e., occurs faster). Slopes can either be classified as weathering limited (weathering occurs slower) or transport limited (transport occurs slower) in which the slower process limits erosion (Wallace, 1997). Weathering-limited slopes are characterized by bare rock exposures at the surface and very steep to vertical gradients. Transport-limited slopes are characterized by sediment covered surfaces (***Figure 3.1***). Since the Ferris Mountains front largely contains faulted quaternary benches of loose, unlithified material, the scarp slopes can be classified as transport-limited slopes (Blair and McPherson, 2009; Mayer, 1984).

Analyzing fault-scarp morphology is conducted by measuring fault-scarp surfaces and modeling their profiles. The profiles of degraded fault scarps resemble the error function, and the degradation process of the slopes is assumed to mirror a sediment diffusive process; therefore, the evolution of slope morphology can be quantitatively evaluated using the diffusion equation (Hanks et al., 1984). To do this, scarp profiles (curves) from several locations along the Ferris Mountains front were measured and fit to generated synthetic profiles. The relationship between scarp height and slope can then be

analyzed and used to estimate the corresponding ages from the morphology of scarps of known ages. Long-term slip rates can also be estimated to infer horizontal deformation.

Initial and Modified Scarp Conditions

Fault scarps generally represent offset of any amount in a planar surface created by vertical or near-vertical motion along a fault. In this study, the fault displacements analyzed are assumed to have occurred as sudden offsets by earthquakes (one or multiple events) as opposed to slow tectonic creep. The different pieces of a fault scarp's anatomy are important to distinguish to understand the initial scarp characteristics after an earthquake and the corresponding modification process as scarp degradation progresses through time.

The Ferris Mountains front holds several fault scarps along a fault zone in which the orientation of faulting is unknown. These faults are steeply dipping (>60 degrees) where the north block in moved downward, and the south block has moved upward. Once the scarps have formed, they immediately begin to change through erosional processes (degradation). The material on the scarp's free face plays a significant role in rate of degradation; in this study, the scarps are held in moderately indurated quaternary regolith benches. With these types of scarp forms, the loose sediment falls from the free face and accumulates on the sloping surface (debris slope) below at the angle of repose (typically 30 to 35 degrees). A more gently sloping wedge at the base of the scarp (wash slope) is consequentially produced; and eventually, the free face disappears and rounding of the scarp crest begins.

Degradation via the Diffusion Equation

Fault-scarp diffusion modeling of eroded, modified profiles can produce a quantitative assessment of the scarp's evolution by determining long-term slip rate and ultimately the age. Multiple faulted surfaces were observed on the Ferris Mountains front that inferred multi-event (composite) scarps. Single-event scarps refer to one surface-rupturing event giving a single age value, as opposed to composite scarps, which refer to several surface-rupturing events giving an average earthquake recurrence interval (measured in thousands of years) (Mayer, 1984). To successfully apply this morphological dating method selection of an appropriate sediment transport model and calibration of its parameters, i.e., determining if a scarp represents one or more events is required (Mattson and Bruhn, 2001). The methodology referencing the modeling of both single- and multi-event fault scarps comes from Hanks et al. (1984) and Hanks (2000) using solutions from Hirano's equation

$$\frac{\partial u}{\partial t} - \kappa \frac{\partial^2 u}{\partial x^2} = 0 \qquad \text{(Equation3.1)}$$

that either assume a single uplift event

$$u(x,t) = a\,\mathrm{erf}\left(\frac{x}{2\sqrt{\kappa t}}\right) + bx \qquad \text{(Equation 3.2)}$$

or a steady-state uplift event

$$u(x,t) = (a + At)\, erf\left(\frac{x}{2\sqrt{\kappa t}}\right) + \frac{Ax^2}{2\kappa}\left[erf\left(\frac{x}{2\sqrt{\kappa t}}\right) - sgn(x)\right] + \left(\frac{Ax}{\kappa}\sqrt{\frac{\kappa t}{\pi}}\right)e^{\left(\frac{-x^2}{4\kappa t}\right)} + bx$$

(Equation 3.3)

and were used for the basis of generating the profiles in Python (https://github.com/seanpolun/pyScarpFit). Diffusion parameters are solved by a grid search, identifying the midpoint of the scarp (defined as x = 0), the upper and lower far-field slope (α), and the vertical offset of the scarp (d). The degrading part of the fault scarp is the convex curvature where x > 0 whereas the aggrading portion is the antisymmetric equivalent (i.e., concave curvature) where x < 0 (Hanks et al., 1984).

3.2 Data Acquisition: sUAV Photogrammetry

sUAV Photogrammetry Data

High-resolution topographic data (DEM) covering the fault scarp in three locations (chosen based on accessibility and visibility of the fault scarp) was collected through low-altitude photogrammetry (***Figure 3.2***). Aerial photos were acquired using a small unmanned system (sUAV a.k.a. "drones") ***Table 3.4*** contains information on the surveys done at each location. The photogrammetric technique for creating these datasets uses Structure-from-Motion (SfM) to estimate 3D structures from 2D image sequences and were also coupled with local motion signals (Fonstad et al., 2013). Unlike classical photogrammetry which utilizes stereoscopic image pairs, SfM solves for the camera's pose and scene geometry simultaneously and automatically while utilizing a highly redundant bundle adjustment based on matching features in multiple overlapping, offset images (3 or more photos). Ground-control points (GCP's) were also placed throughout

the surveyed area and measured through a terrestrial photogrammetric technique using RTK and long exposure GPS equipment for post-processing elevation precision.

3.3 Scarp Profiling

Scarp Profiling

Five scarp profiles were extracted along the fault system from each surveyed location to elucidate geomorphic and tectonic evolution (***Figure 3.3***). These scarps represent the culmination of single- and multi-event faulted surfaces based on relative parameters (grouped together with similar vertical displacement components and amount of degradation). A one-dimensional, non-linear sediment transport (scarp degradation) model was applied to these profiles and calibrated using associated parameters of mass diffusivity (rate of degradation) and vertical displacement (throw) obtained from the regional slope, from the maximum displacement. To do this, the sUAV photogrammetry data were converted to pointCloud data (georeferenced points) and aligned to the correct elevation and spatial orientation using the GCP locations. Information on these surveys can be found in ***Table 3.4***. Using the Metashape software, (resolution) DEM models were produced (***Figure 3.4d***). From these models, several pairs of points (X and Y values as UTM coordinates) on either side of the SGMFS were extracted to produce cross-sectional elevation profiles.

Diffusivity Calibration

Using the ages for Bull Lake and Pinedale surfaces given by Phillips et al. (1997), the value for mass diffusivity can be calibrated more precisely. Soil characteristics were used to age corelate surfaces along the Ferris Mountains front with Bull Lake and Pinedale type surfaces (Geomatrix Consultants inc., 1988). Cosmogenic age data for

Bull Lake constrain its age to be >130 – 95 ka. Pinedale cosmogenic data constrain its age to be 23-16 ka. (Phillips et al. 1997). Assuming diffusivity of the region is between 1.0-0.9 and 2.0 +/- 0.4 (taken from Lost River, Idaho fluvial terrace risers, southwest Montana respectively, Hanks, 1984). By dividing the κt value from the scarp models by the ages given from correlated surfaces, a more precise value of κ is computed. From this an average κ value for mass diffusivity is determined to be 0.97 +/- 0.28

3.4 Results

The throw (H) and degree of degradation (κt) are estimated for both single- and multi-event scarps from the degradation models. The diffusivity constant is then applied to calculate ages (t) of the faulted surfaces. Composite scarp data are used to calculate earthquake recurrence intervals and uplift rates from each throw component. Single-event scarp data, however, are used to calculate the timing of the last surface-rupturing event and corresponding earthquake magnitudes (Wells and Coppersmith, 1994).

The best-fit profiles for single- and multi-event scarps within the Ferris Mountains segment also include uncertainties [σ] on the fault scarp's throw, κt, κ, age, and deformation rates. Calculations for each single- and multi-event profile with corresponding uncertainties are displayed in the tables below.

Single-Event Fault Scarp Profiles

None of the scarps observed in this location are interpreted to be single event scarps. Based on empirical relationships between maximum surface displacement (MD) of normal faults and moment magnitude (M), the log-linear regression from Wells and Coppersmith (1994),

$$M = 6.96(\pm 0.04) + 0.74(\pm 0.07) * \log(MD) \quad \text{(Equation 3.4)}$$

is used to approximate the magnitudes on each scarp, where MD is interpreted as throw. Using the approximated range magnitudes for the most recent earthquake along the Ferris Mountains segment of 6.4 - 6.9 (Geomatrix Consultants inc., 1988), the expected throw on the scarps would range from approximately 0.17 – 0.93 meters in height. This measure is significant at a 95% confidence interval (Wells and Coppersmith, 1994). All scarps observed along the Ferris mountains front are larger than this maximum value for throw, and therefore the scarps must

represent multiple events.

Multi-Event Fault Scarp Profiles

Composite scarp models from Cherry Creek, Pete Creek, and Arkansas Creek were analyzed using a steady state model (Hanks et al., 1984) these scarp profiles range from 2 to 4.0 meters in vertical displacement. Q2 surfaces are interpreted as being Bull Lake in age while surface Q3 historically has been correlated to being post Pinedale in age (Geomatrix Consultants inc,, 1988). The κt value, given from the degradation model, can then be divided by mass diffusivity yielding the age ranges of the faulted surface. Faults in surface Q3 at Cherry Creek and Pete Creek date to be 16 +/- 2.4 ka. While surface Q2 at the same locations are 95 +/- 14.25 ka. The only age estimate for surface Q1 comes from Arkansas Creek which dates to 201 +/- 133 ka. To calculate corresponding dip slip and extension rates via trigonometry, a range of slope angles is assumed from 55 to 80 degrees (55 degrees being an average for transport-limited slopes; Wallace, 1977). Long term slip rates from Cherry, Pete, and Arkansas creek are Shown

to range from 0.01-0.05 mm/yr. While horizontal extension rates are shown to range from 0.01 – 0.03 mm/yr.

Table 3.1 Surface Q3 data

Surface	**Cherry Creek Q3**	**σ**	**Pete Creek Q3**	**σ**
H(m)	2	+/- 0.04	2.08	+/- 0.04
kt(m2)	17.2	+/- 1.4	16.1	+/- 1.6
k(m2/kyr)	0.97	+/- 0.28	0.97	+/- 0.28
t(years)	16000	+/- 2400	16000	+/- 2400
Uplift (mm/yr)	0.125	+/- 0.03	0.13	+/- 0.03
Exten. (mm/yr) 55 deg.	0.03	+/- 0.02	0.03	+/- 0.02
Exten. (mm/yr) 80 deg.	0.01	+/- 0.004	0.01	+/- 0.003
Dip Slip 55 deg.	0.005	+/- 0.003	0.005	+/- 0.003
Dip Slip 80 deg.	0.01	+/- 0.003	0.05	+/- 0.02

Table 3.2 Surface Q2 data

Surface	**Cherry Creek Q2**	**σ**	**Pete Creek Q2**	**σ**
H(m)	2.78	+/- 0.04	2.4	+/- 0.06
kt(m2)	81.6	+/- 7.2	73.4	+/- 8.7
k(m2/kyr)	0.97	+/- 0.28	0.97	+/- 0.28
t(years)	95000	+/- 14250	95000	+/- 14250
Uplift (mm/yr)	0.03	+/- 0.006	0.03	+/- 0.006
Exten. (mm/yr) 55 deg.	0.01	+/- 0.003	0.01	+/- 0.003
Exten. (mm/yr) 80 deg.	0.002	+/- 0.001	0.002	+/- 0.001
Dip Slip 55 deg.	0.001	+/- 0.0004	0.001	+/- 0.001
Dip Slip 80 deg.	0.01	+/- 0.005	0.01	+/- 0.005

Table 3.3 Surface Q1 data

Surface	**Arkansas Creek Q1**	**σ**
H(m)	3.54	+/- 0.12
kt(m2)	167.9	+/- 34.8
k(m2/kyr)	0.97	+/- 0.28
t(years)	210053	+/- 133309
Uplift (mm/yr)	0.02	+/- 0.02
Exten. (mm/yr) 55 deg.	0.02	+/- 0.001
Exten. (mm/yr) 80 deg.	0.004	+/- 0.002
Dip Slip 55 deg.	0.001	+/- 0.00005
Dip Slip 80 deg.	0.02	+/- 0.01

Table 3.4 sUAV Survey Information

Survey Location	# Of GCP's	# Of flights	# Of photos	# Of points	Survey Area (m^2)
Cherry Creek	4	3	1077	253469760	162292
Pete Creek	3	3	625	90419453	298915
Arkansas Creek	4	1	104	83875399	63909

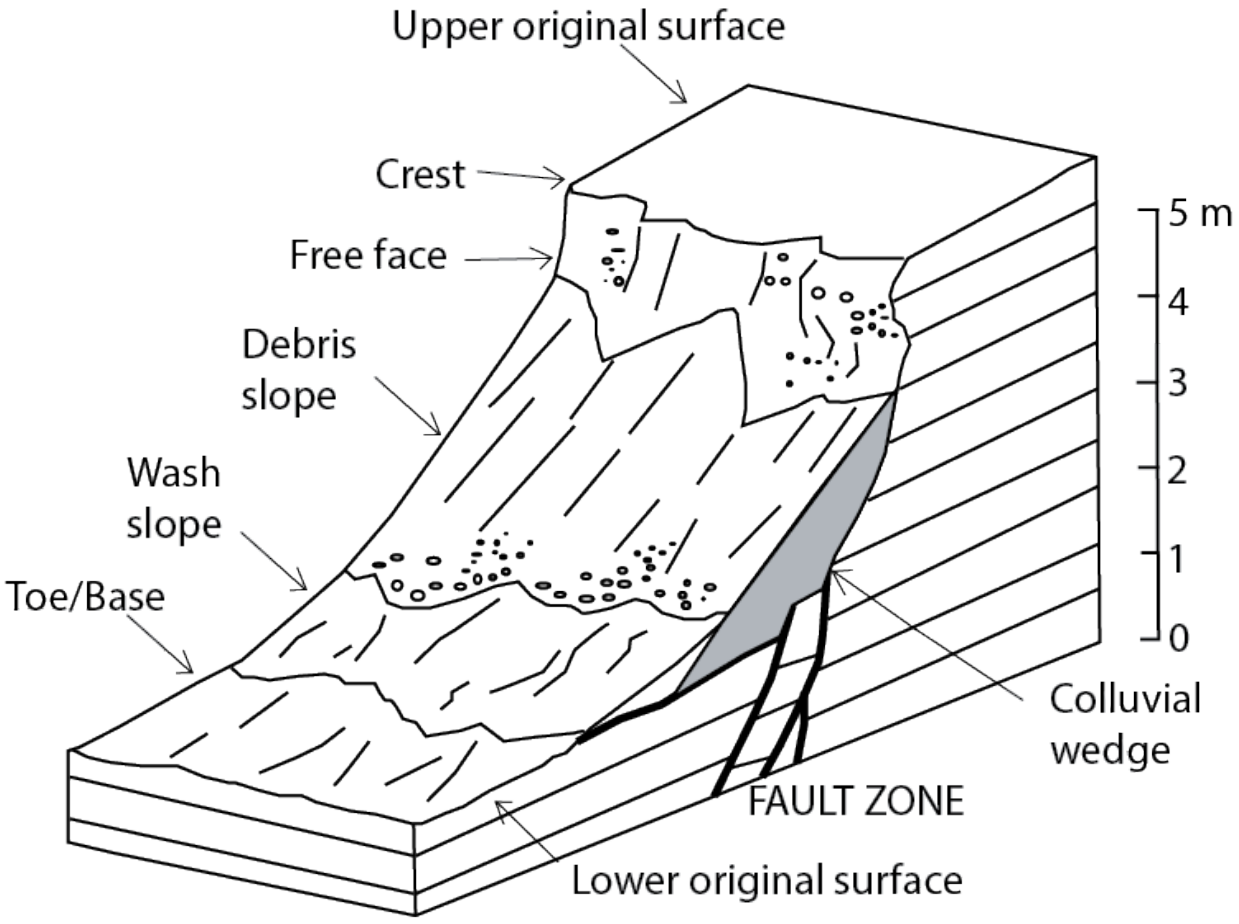

Figure 3.1 – Scarp anatomy from Wallace (1977), showing degradation of a transport limited scarp.

A

Figure 3.2 A – Digital elevation models of each field location superimposed on a Google Earth Pro overlay at Arkansas Creek field location. See ***figure 2.3A***.

B

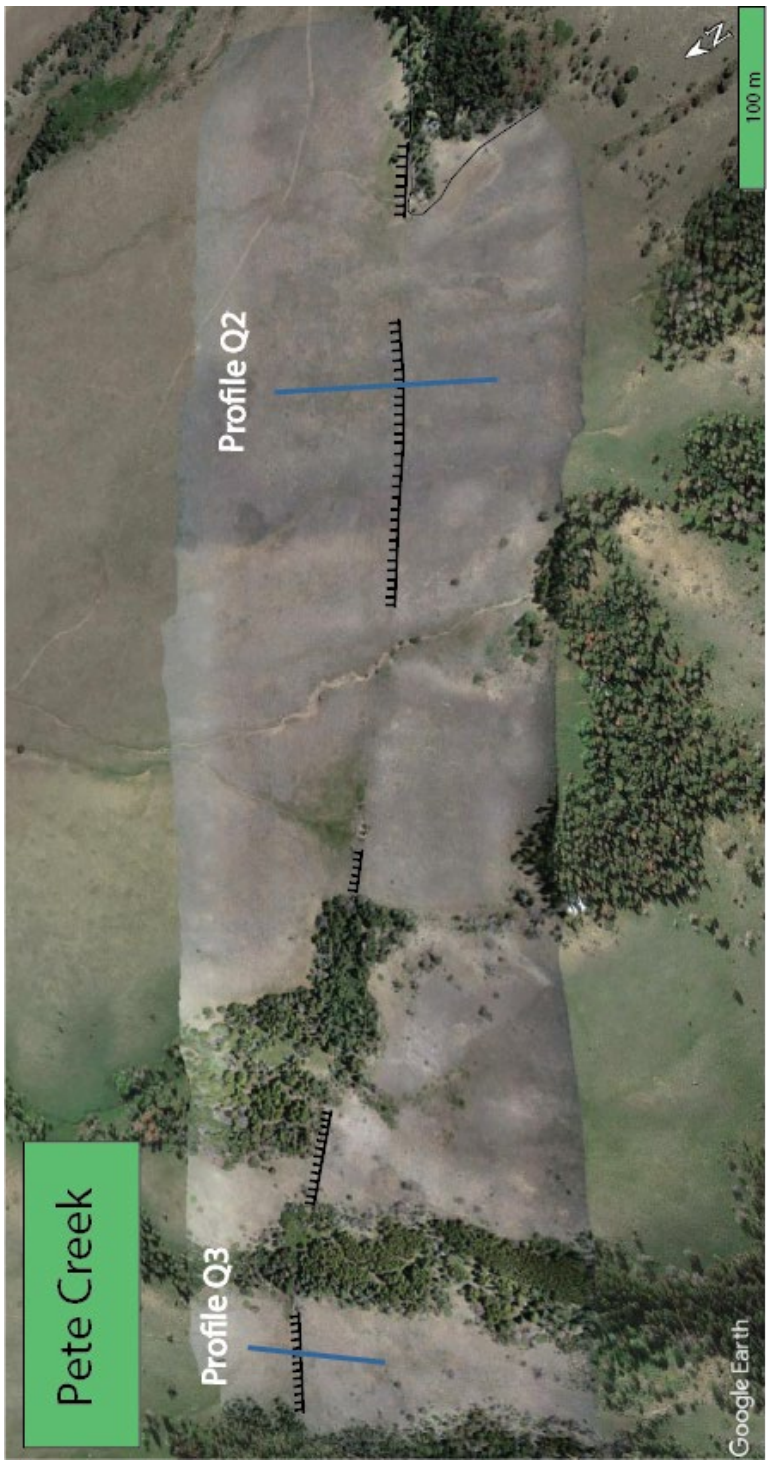

Figure 3.2 B – Digital elevation models of each field location superimposed on a Google Earth Pro overlay at Pete Creek field location. See ***figure 2.3B***.

C

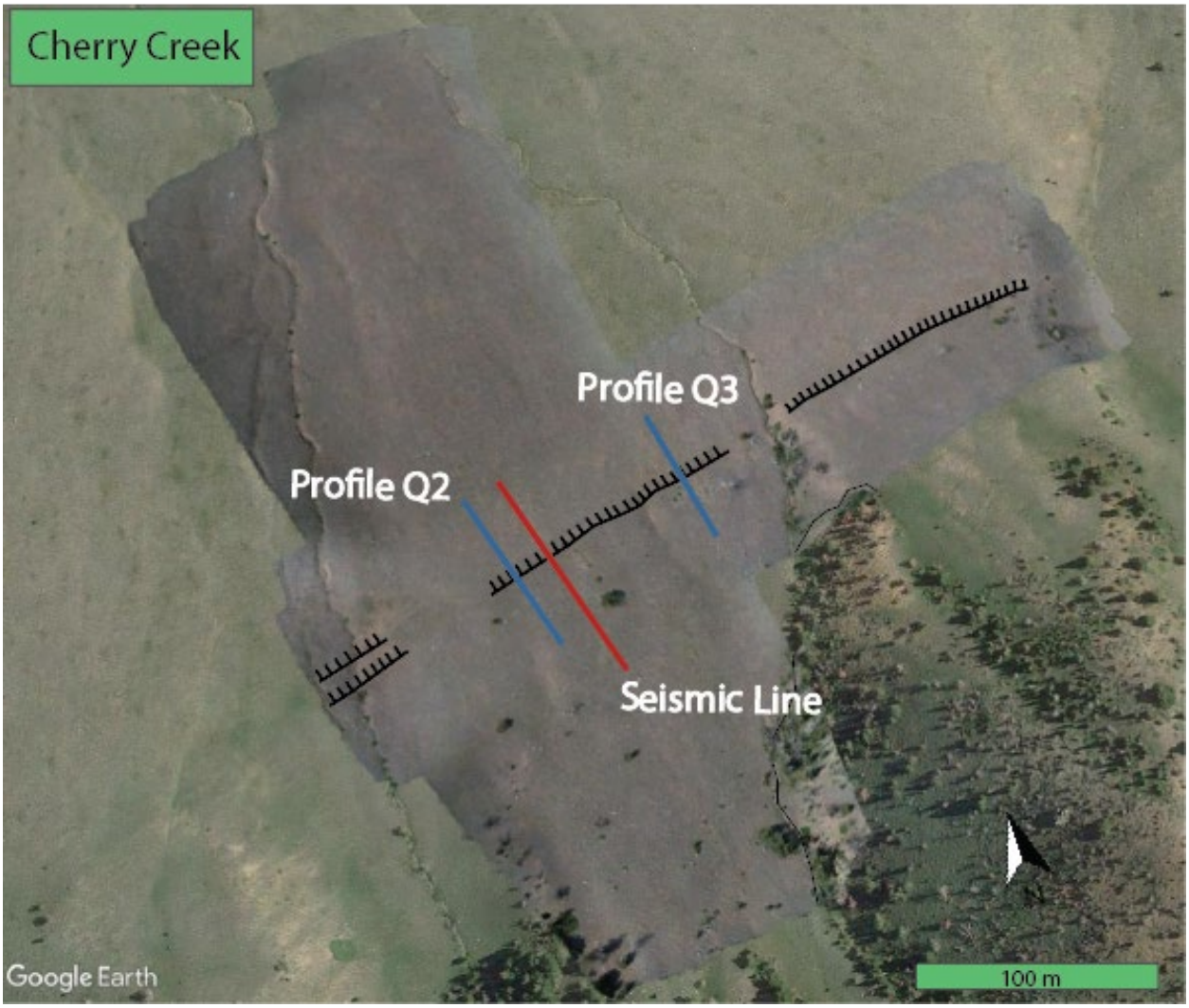

Figure 3.2 C – Digital elevation models of each field location superimposed on a Google Earth Pro overlay at Cherry Creek field location. See ***figure 2.3C***.

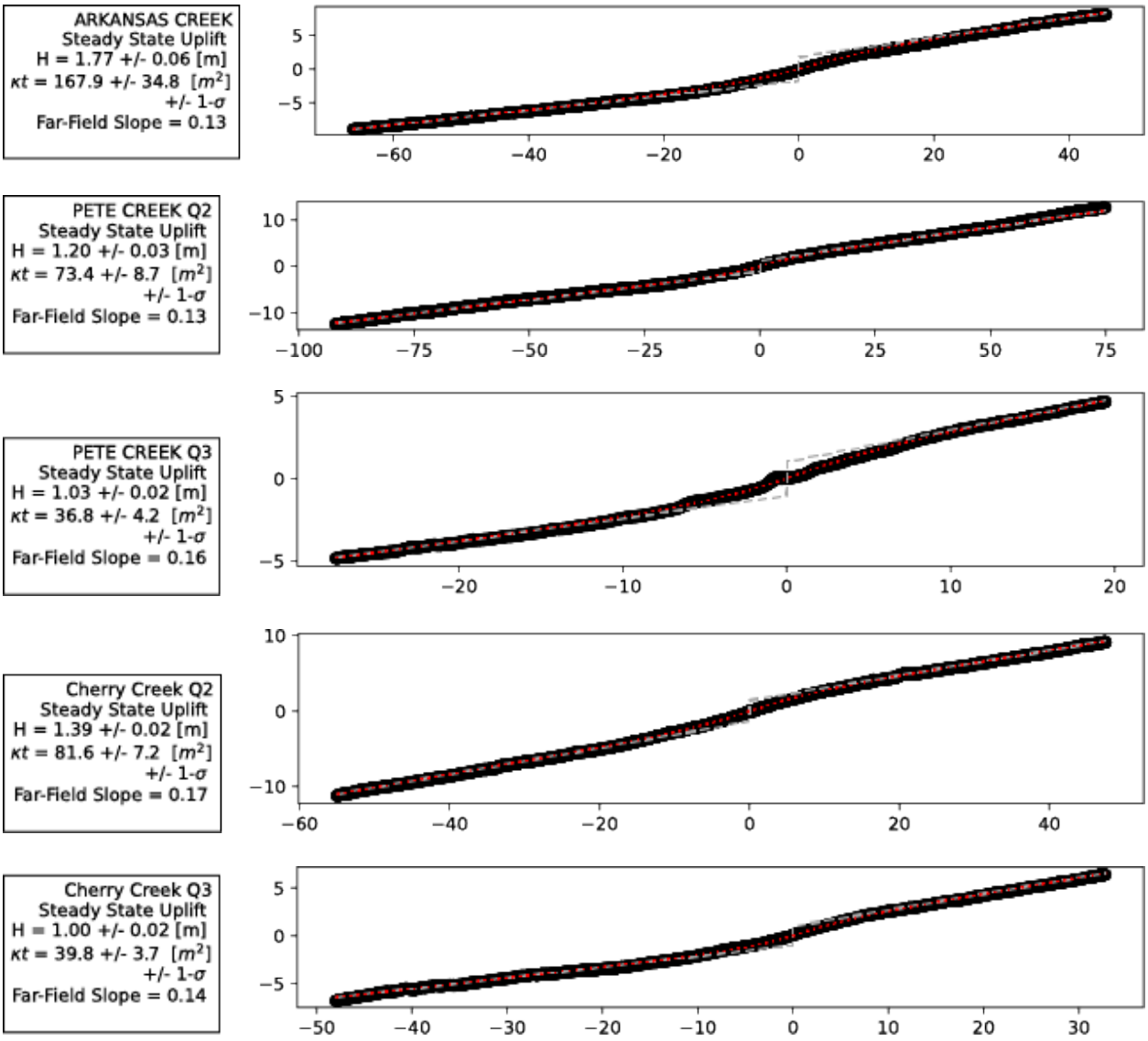

Figure 3.3– Scarp profiles and degradation models from the Ferris mountains front, H here is denoted as the scarp half-height

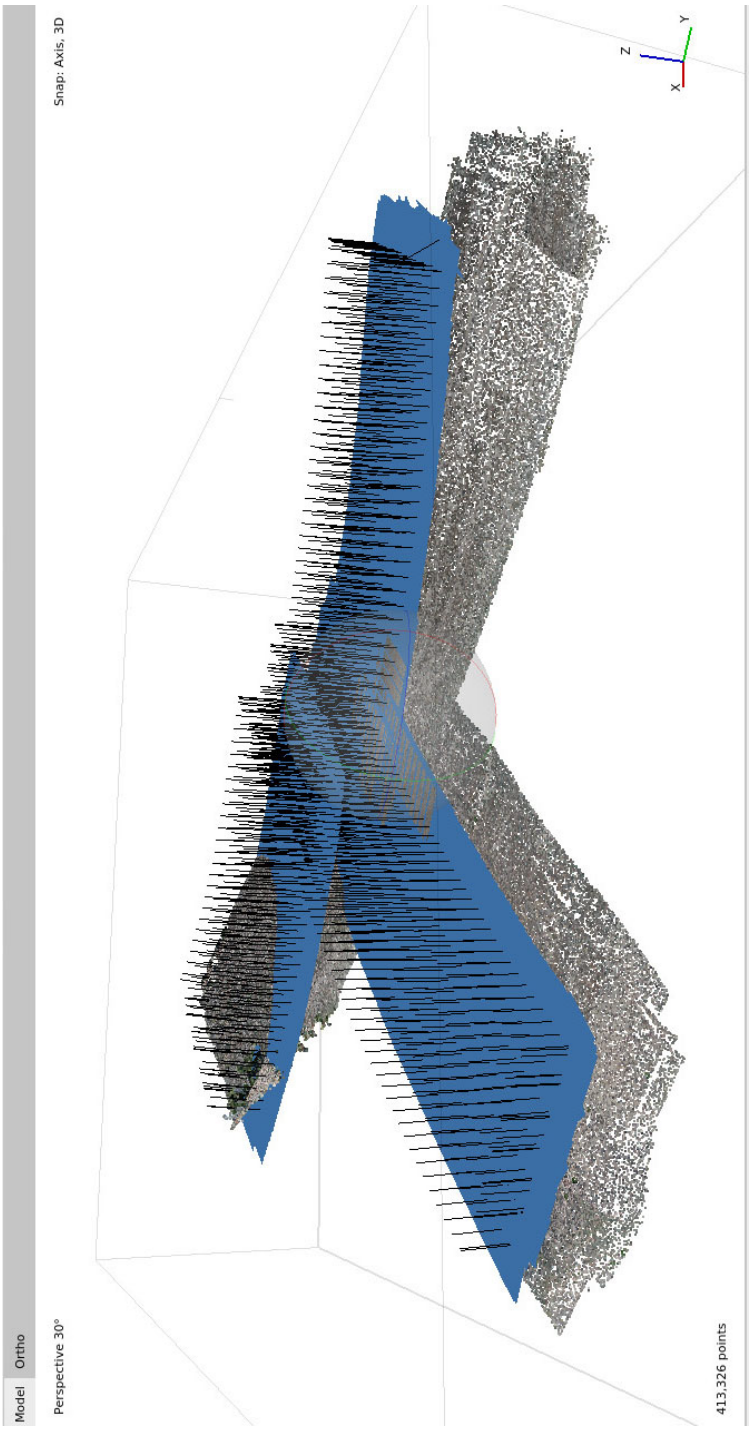

Figure 3.4 – Metashape aligned photos from Cherry Creek which were used to create the Digital elevation models

Figure 3.5 – Photograph of Dr. Sean Polun about to takeoff for survey flights at the Pete Creek location.

Chapter 4: Shallow Geophysics

4.1 Overview and basic idea

Refraction and reflection seismology methods were utilized to acquire subsurface (e.g., depth, geometry) data for the Ferris Mountain segment of the SGMFS at the Cherry Creek field site (***Figure 3.2C***). The detailed images produced from these methods can be used to identify the underlying structural geometry and fault characteristics.

The concept behind these methods is derived from the principal of elastic waves (seismic waves propagate though the earth as elastic waves). From their surface source, seismic waves are transmitted into the earth. Therein most of their energy is refracted or reflected at each lithological interface (any remaining energy is absorbed). Lateral and depth variations can be distinguished through a physical and relevant parameter of seismic velocity because these waves travel with different velocities in different lithologic layers. With the goal being to analyze the depth and geometry of potential subsurface features, an estimation of the seismic velocity of the rocks is needed.

The datasets acquired through this survey consist of a series of travel time versus distance (two-way travel time). These datasets allow for the reconstruction of the refracted and reflected wave paths, since most of the sound from the source is returned back to the surface, i.e., measuring the time between the initial sound from the source and the returned echo. For both seismic wave types, the difference in travel time depends on the physical properties (elastic parameters) of the material in which the waves are traveling though, as well as the attitudes of the geologic layers.

The geophysical assessment of the study area involved two seismic survey approaches – a 112-meter fixed spread refraction survey and a 112-meter fixed spread

reflection survey. For both surveys a seismic Betsy gun with 8-guage shells was manually operated as the source and 56 vertical components, 40-Hz geophones (electro-magnetic devices), were placed in the ground surface and acted as receivers.

4.2 Seismic refraction

The seismic refraction survey took place at Cherry Creek, the westernmost field site, ran perpendicularly across the fault scarp and extended 112 meters in length. The approach involved a fixed spread ("common offset") array in which the 56 geophones used were placed with a predetermined 2 meter spacing. This geophone array was overlain with the shot (where the Betsy gun seismic source was shot) locations with a predetermined 6 meter spacing (***Figure 4.1***).

Geophone and shot spacing were verified along the seismic lines prior to data collection using flags and measuring tapes. Holes for the shots were then dug approximately 0.5 meters in depth with a power auger, needed to get through the rocky soils. These holes helped to accommodate the blast from the Betsy gun and retain as much energy as possible into the ground. Each geophone was installed manually by first digging a small hole in the rocky soils with a rock pick and then pressing the 3-inch receiver spike into the ground to establish a firm connection with the ground surface, this ensured a good coupling to the ground surface so that seismic energy from the ground was transferred directly to the geophone. Each geophone was then connected to a digital recorder (Geometrics Seismograph), via a multi-channel data cable. Tap tests were done at each geophone while observing the signal strength display on the display screen of the recording unit to confirm that each geophone was in its proper place and that the orientation of the communication cable was correct. Once the recording unit had been

calibrated, we began the survey upslope at the 96-meter source location and worked moving downslope toward the graben interior, ending at the 234-meter source location. One shot impact was done at each location to collect data; if the seismograph displayed too much noise, or there was a false trigger, the shot was redone replacing the previous shot impact data.

Data Processing

Travel times of refracted P- and S- waves change as they pass through each medium changing the angle of refraction (e.g., V_1 and V_2 layers) which indicates change in speed and wavelength. The principal portion of these wave paths are along the interface between each layer and therefore, approximately horizontal. Travel times of refracted wave paths are therefore interpreted in terms of depth to subsurface interfaces and speeds at which the waves travel within each layer.

SeisImager/2D refraction software was used to integrate the refraction modeling and interpretation. Raw field data records were first imported as individual files into the PickWin module, with each record demonstrating the impact along the seismic profile from a single shot location. P-wave shot gathers were compiled and the first-arrival times (first breaks) were picked; no filters were necessary in the picking. The P-wave first arrivals were all measured within 0.1 seconds. The P-wave first arrivals were measured for every corresponding geophone (56) from each shot point (24) along the profile. This resulted in a total of 1,344 first arrivals used to develop the P-wave velocity model.

These picks were combined into one file that was then imported into the Plotrefa module. Inflection points along the crossover distances were then selected to mark

changes in slope which represent a change in seismic wave speed (V_1 layer to V_2 layer). Vertical variations between interfaces (time inversion analysis) were then applied with field measured elevation points (topographic profile) which were also imported to ensure accurate topographic profiling. The time inversion model served as the basic model from which an initial velocity model was generated giving the tomographic inversion. The final P-wave seismic-refraction tomography model was generated to map the lateral variations in P-wave velocity (***Figure 4.2 & 4.3***).

4.3 Seismic Reflection

Seismic reflection surveying took place along the same profile as the seismic refraction survey and was collected during the same time following the same parameters and methods listed in the previous section. In this approach the same dataset from the fixed spread survey was used. The purpose of using the data from the fixed spread for the reflection profiling was to observe the shallow reflectors near the fault plane to image the fault geometry and verify the fault location with the seismic refraction model. Since Precambrian granite bedrock exists near the surface and there are minimal deep reflectors from which geometry can be imaged.

Data Processing

The time it takes for P- waves to travel from the source location to the subsurface reflector and back to the surface is recorded as a two-way travel time. For the subsurface layers to reflect seismic waves back to the surface there must be a change in the acoustic impedance (z), which the product of the layer's seismic velocity (v) and density (ρ) (such that $Z = Vi\rho i$ for the *i*th layer), between layers. The sampled point of reflection is half

the distance from the source to the receiver, and the spacing between sampled reflection points is half the geophone spacing.

The “Seismic Unix” reflection software was used to create common depth point (CDP) stacks to identify shallow reflectors below the fault scarp and to image the geometry of faulting. Raw data records were first imported as individual files into Visual SUNT and converted into the appropriate format of a single file containing all the shot gathers. Next the traces that failed during recording were muted to remove them from further processing. The data was run through two different bandpass filters to compare the clarity results. The first bandpass filter was between 60 and 80 Hz, and the second between 45 and 65 Hz.

The ground roll and first arrivals were then muted from each shot gather using the interactive SUMUTEX 1.0 program. By doing this the p wave signal from the reflectors is left while the noise from the surface waves is removed making imaging the shallow reflectors clearer. After all the shot gathers had been muted the geometry of the array was input into Visual SUNT and data was then sorted into CDP gathers. Using a constant velocity stack, the CDP gathers were stacked so that we could choose which of the stacking velocity file offered the best resolution of the reflectors for the 60-80 Hz bandpass filtered data, stacking velocities in steps of 100 m/s were generated between 800-2700 m/s. For the 45-65 Hz bandpass filtered data, stacking velocities in steps of 100 m/s were generated between 800-3000 m/s. The clearest stacking velocity, with respect to signal to noise clarity, was then chosen to be used to estimate the normal move out (NMO) correction. The best resolution of shallow reflectors was the 1000 m/s file from the 60-80 Hz bandpass filtered data. The 45-65 Hz bandpass filtered data stacked

CDP velocities were all deemed to be of lower quality due to the signal to noise ratio (***Figure 4.4***). The stacked CDP section was then depth converted to produce the final seismic reflection model mapping the lateral variations in acoustic impedance (***Figure 4.5***).

4.4 Results

The refraction survey permitted imaging depths of approximately 46 meters below the surface. P-wave velocity modeling reveals the underlying structure (***Figure 4.6***). In the upper 10 meters velocities range between 730 m/s and ~2450 m/s on the upslope portion of the profile. Downslope to the north, the upper 10 meters is dominantly 730 – 960 m/s. Therefore, the tomography model displays a layer of velocity (<729 – 1500 m/s) material interpreted as sands and gravels. The water table is marked to be present at about 8 meters depth where the seismic velocity increases to 1500 m/s. With increasing depth (15-45 meters) the velocities range from 1760 up to 2676 m/s at the base of the model. This is interpreted as the Tertiary Split Rock Formation (conglomerate). The paleoseismic trench log CC-1 indicates that bedrock should be present between 3- and 4-meters depth along the seismic profile, this is however not the case in the refraction tomography. It is most likely that the feature marked as bedrock by Geomatrix Consultants inc, (1988) in their paleoseismic trench log is in fact a large boulder that had fallen down the hillslope and was subsequently covered by quaternary sediments. If the Precambrian Granite did exist at such shallow depths, a much higher velocity would be expected at shallower depths along the profile. For igneous rock a seismic velocity would be expected to between 4000- and 5000- m/s. These speeds aren't approached at

all along the length of this profile and thus the granite is too deep to be imaged with this method.

At ~170 meters on the survey the distribution is segmented by the fault plane. ~ 15 meters depth between the 170 and 182 meter mark the velocities sharply drop down from 2790 m/s to 2450 – 1800 m/s and is interpreted as northeast dipping normal fault. The amount of throw on this fault is variable, here it is measured to be between 13- and 10- meters. Between the 192- and 202-meter marks another velocity change is observed at ~25 meters depth where velocity decreases from 2450 – 1875 m/s, this is interpreted as a second step of the fault that is imaged at depth. This step does not appear to be surface rupturing and is interpreted to be synthetic to the first fault step. The amount of displacement on this fault appears to be small as the larger step further down the profile is not indicative of the amount of displacement because there is not sufficient sampling at that depth.

The reflection survey permitted imaging depths of up to 75 meters before signal becomes incoherent. At ~ 60 meters distance on the reflection survey the layered reflectors are shown to be warped downward and a subtle displacement is observed at the point of inflection. This matches the placement of the fault on the tomographic model. Another subtle warp in reflectors is present at ~70 meters on the profile interpreted here as the second synthetic fault plane that is not surface rupturing. The faults here is steeply dipping with a direction element to the northwest at approximately 83°. In the footwall the reflectors are relatively horizontal with coherent reflectors identified to depths of ~50 meters. In the hanging wall the reflectors exhibit a moderate dip to the north that persists up to ~75 meters depth before coherence is lost.

Rolling – spread

A second seismic line was shot at cherry creek using a rolling spread convention where 16 shot gathers were recorded keeping a 6-meter shot spacing and a 2-meter geophone spacing. Offset from the first geophone was 96 meters to the last shot with the first geophone positioned at station 144 m. Only one role of 24 geophones was done on this survey due to a limited time frame. Upon processing this data to view preliminary results no coherent reflectors appeared along the profile. This particular dataset had a lot of noise and thus filtering was needed, however, after filtering the signal to noise ratio was still too great for any subsurface structure to be successfully imaged. No useful data was able to be extracted to enhance the overall interpretation of the subsurface at this location.

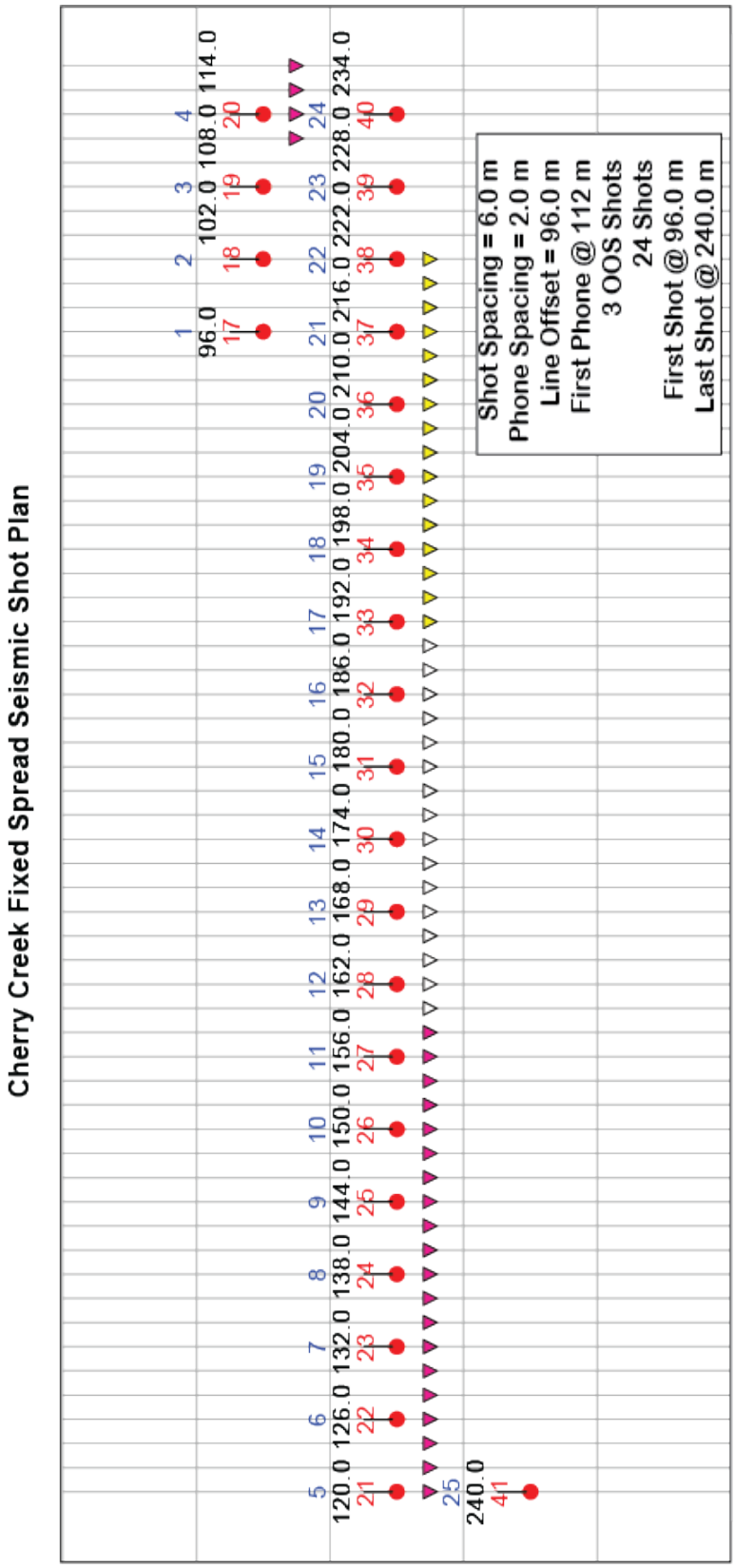

Figure 4.1 – Shot plan for the fixed spread seismic survey done at Cherry Creek

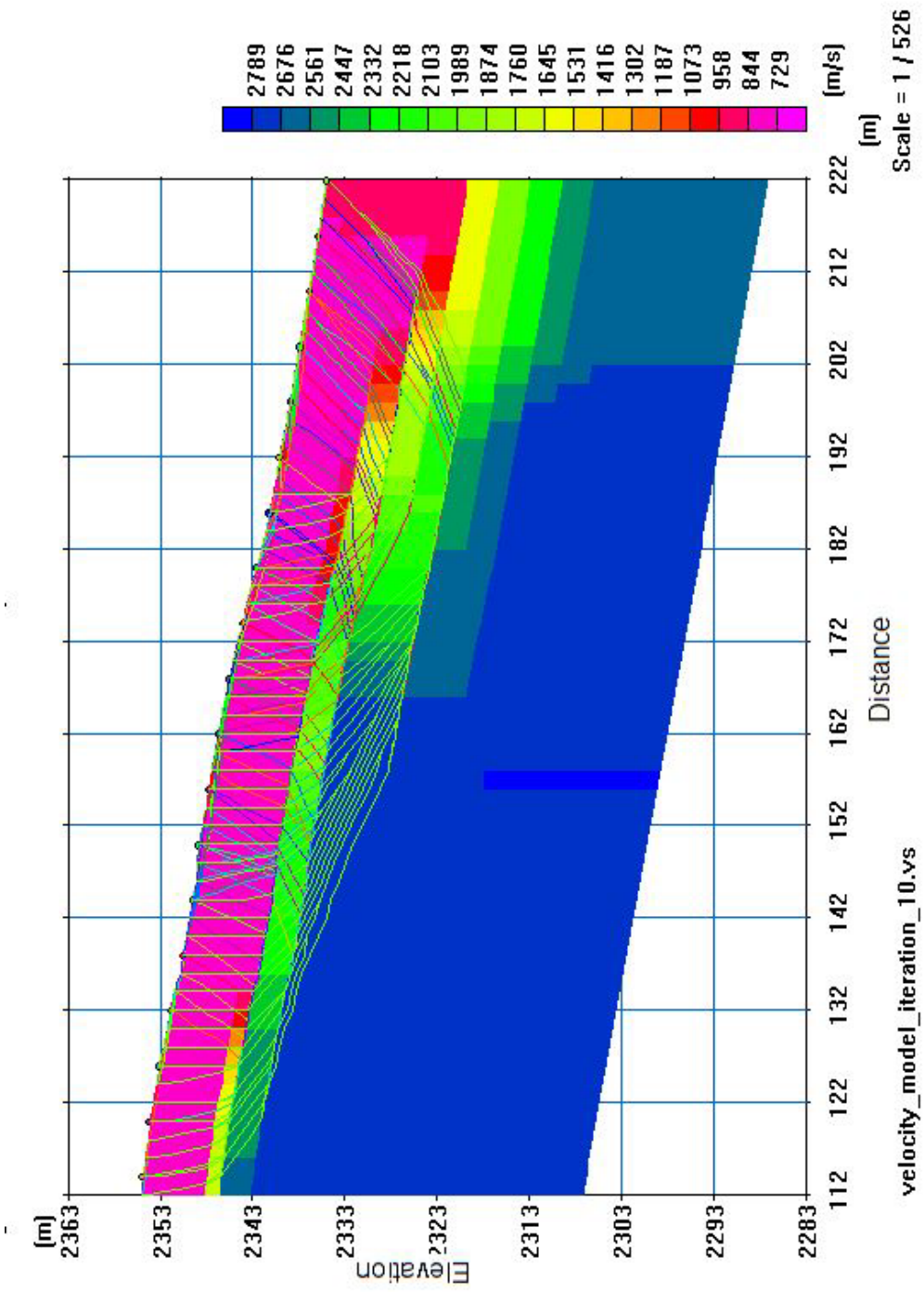

Figure 4.2 – Refraction tomography with ray tracing turned on to show the depth of sampling.

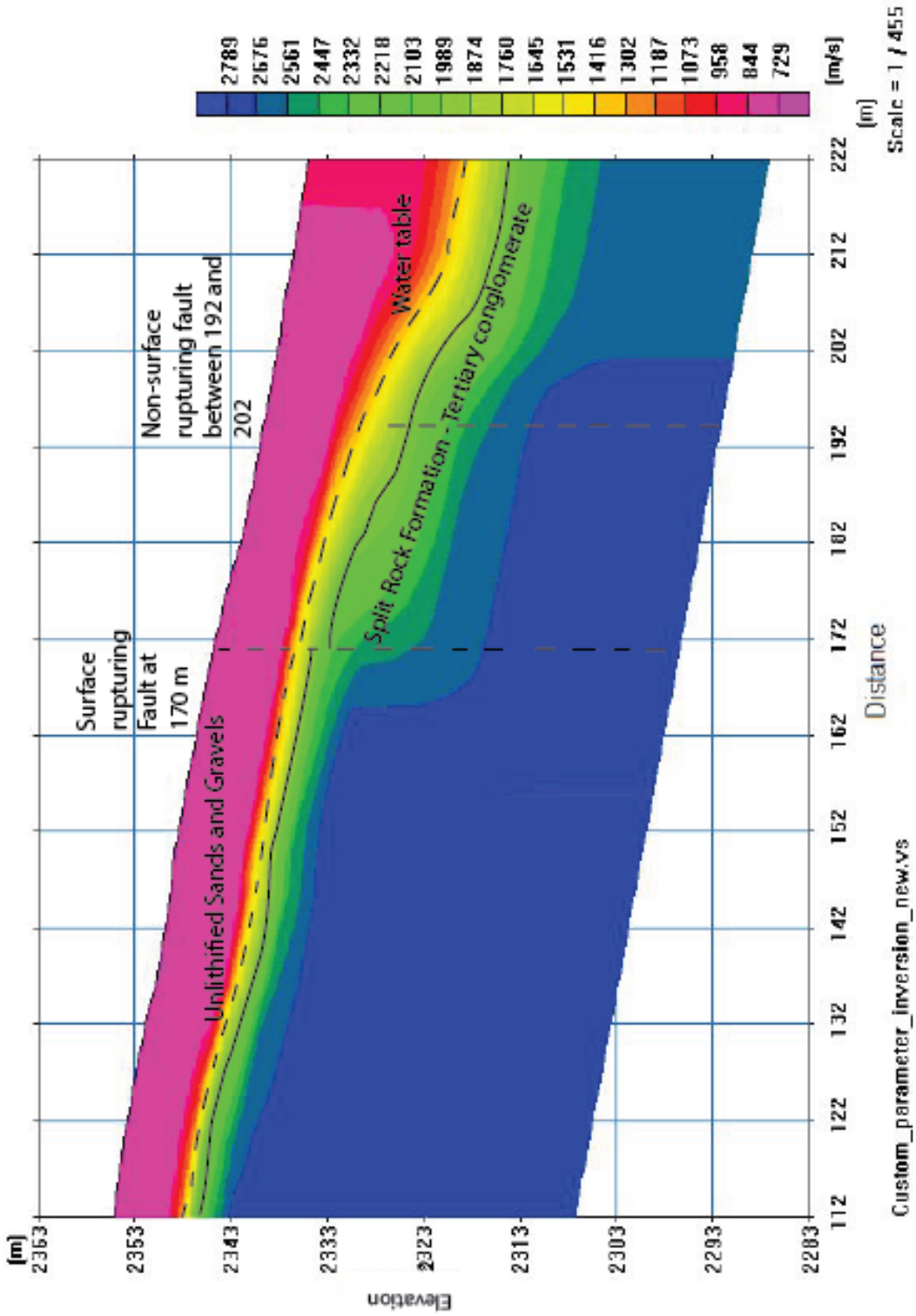

Figure 4.3 – Tomographic model of the SGMFS at Cherry Creek, location of the fault plane is ~170 meter along the survey line. RMS of 2.13 is reported for this model.

A

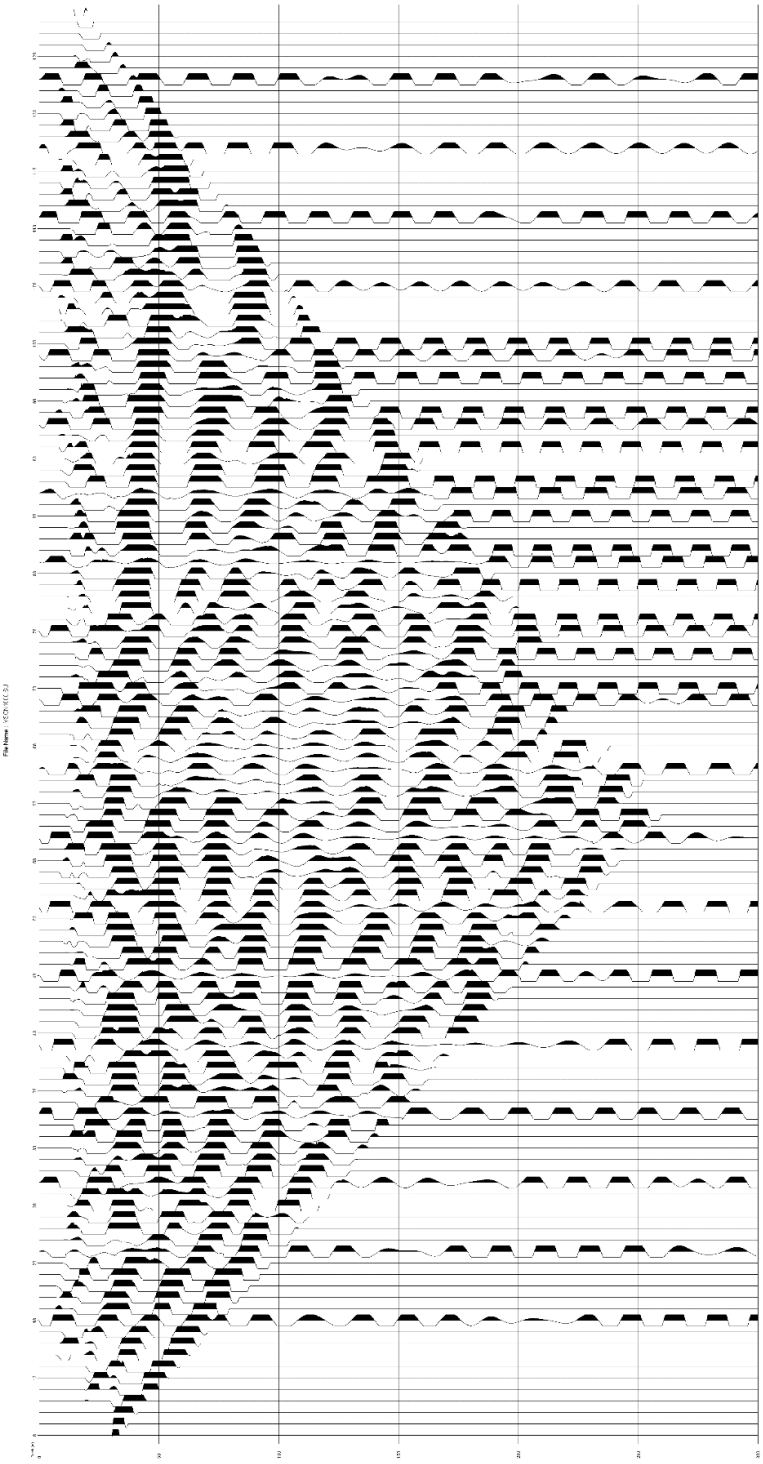

Figure 4.4 A – Non-depth converted reflection data comparing 1000 m/s velocity stack of data ran with the 45-65 Hz bandpass filter showing poor reflector coherence.

B

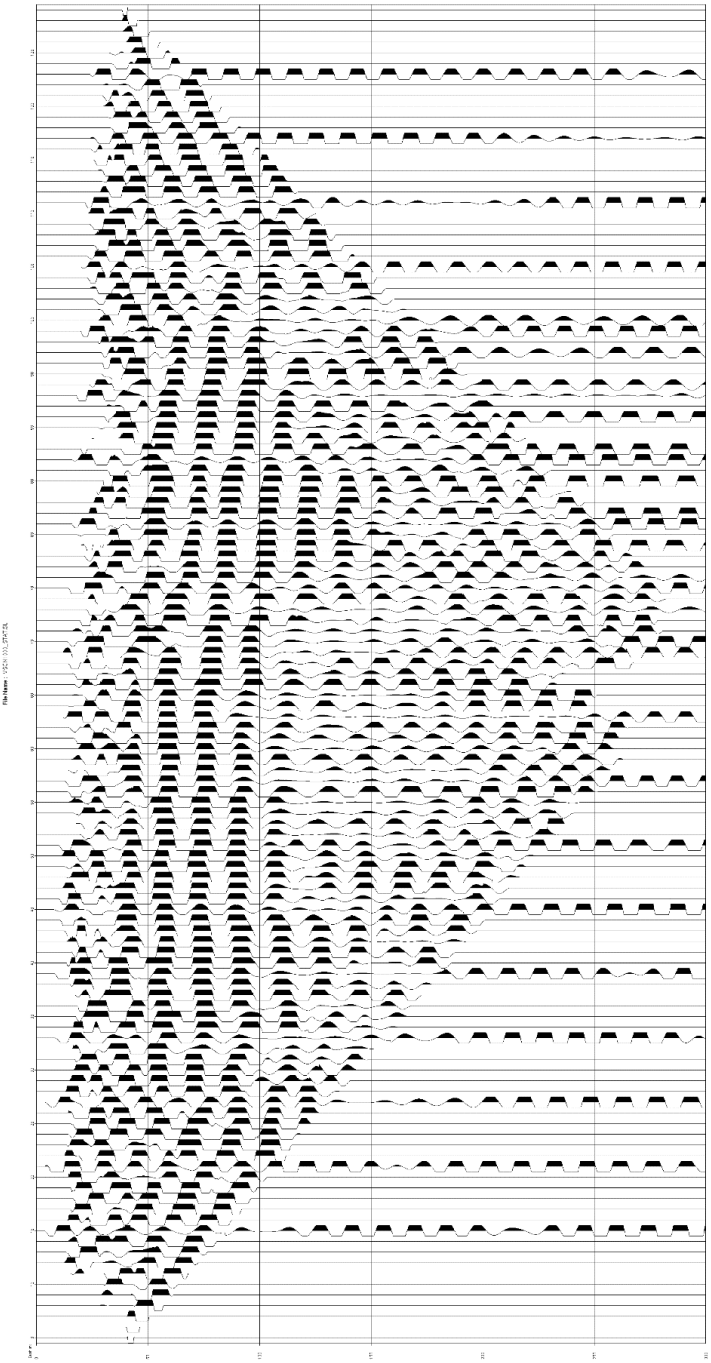

Figure 4.4 B – Non-depth converted reflection data comparing 1000 m/s velocity stack of data ran with the 60-80 Hz bandpass filter to show quality of reflector coherence.

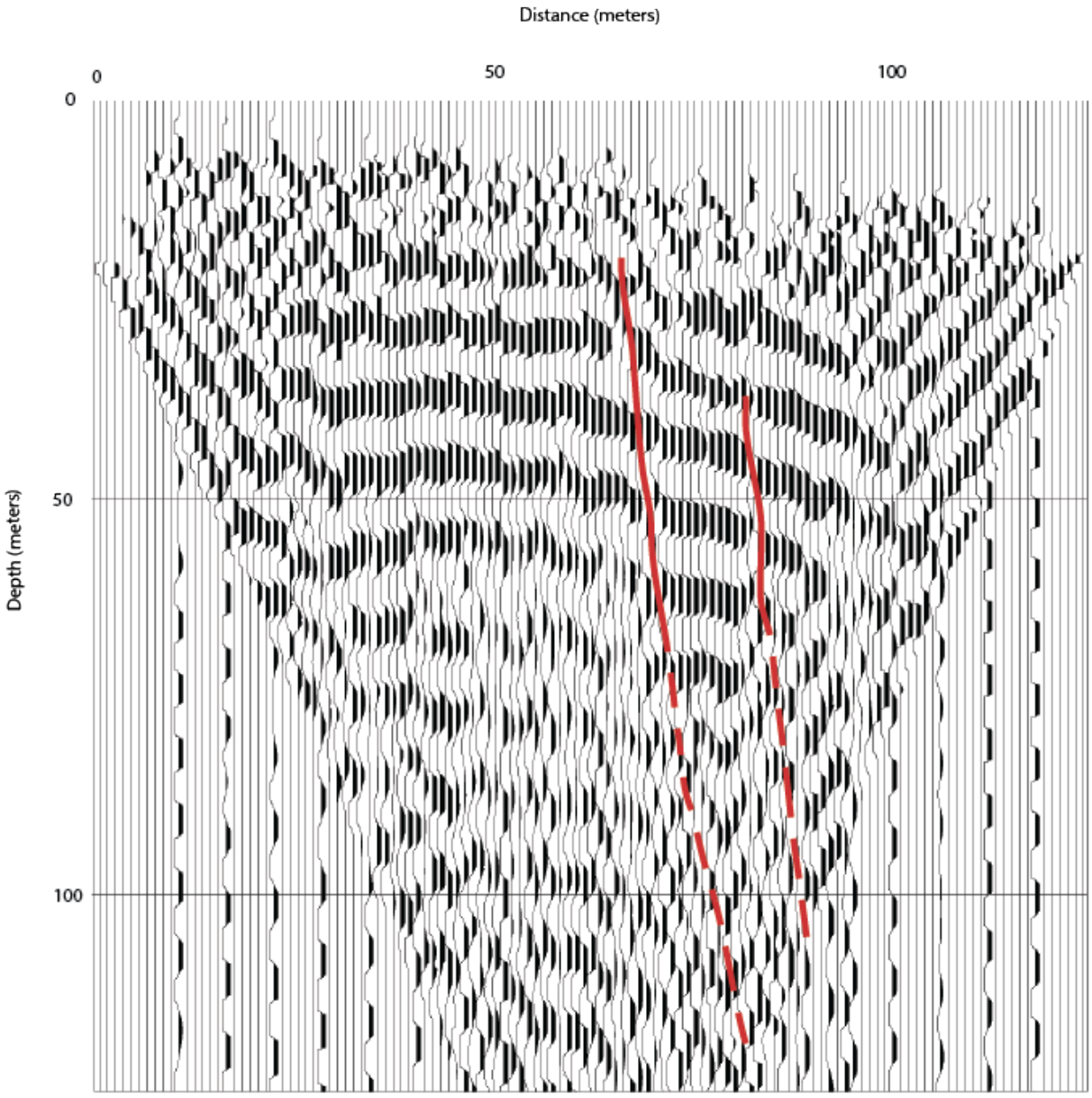

Figure 4.5 – Depth converted data from the 1000 m/s velocity stack showing the reflector warp at approx. 60 meters from the first geophone. Dip here is interpreted to be basin-ward at 83° indicating normal faulting. Dashed line where fault is inferred at depth.

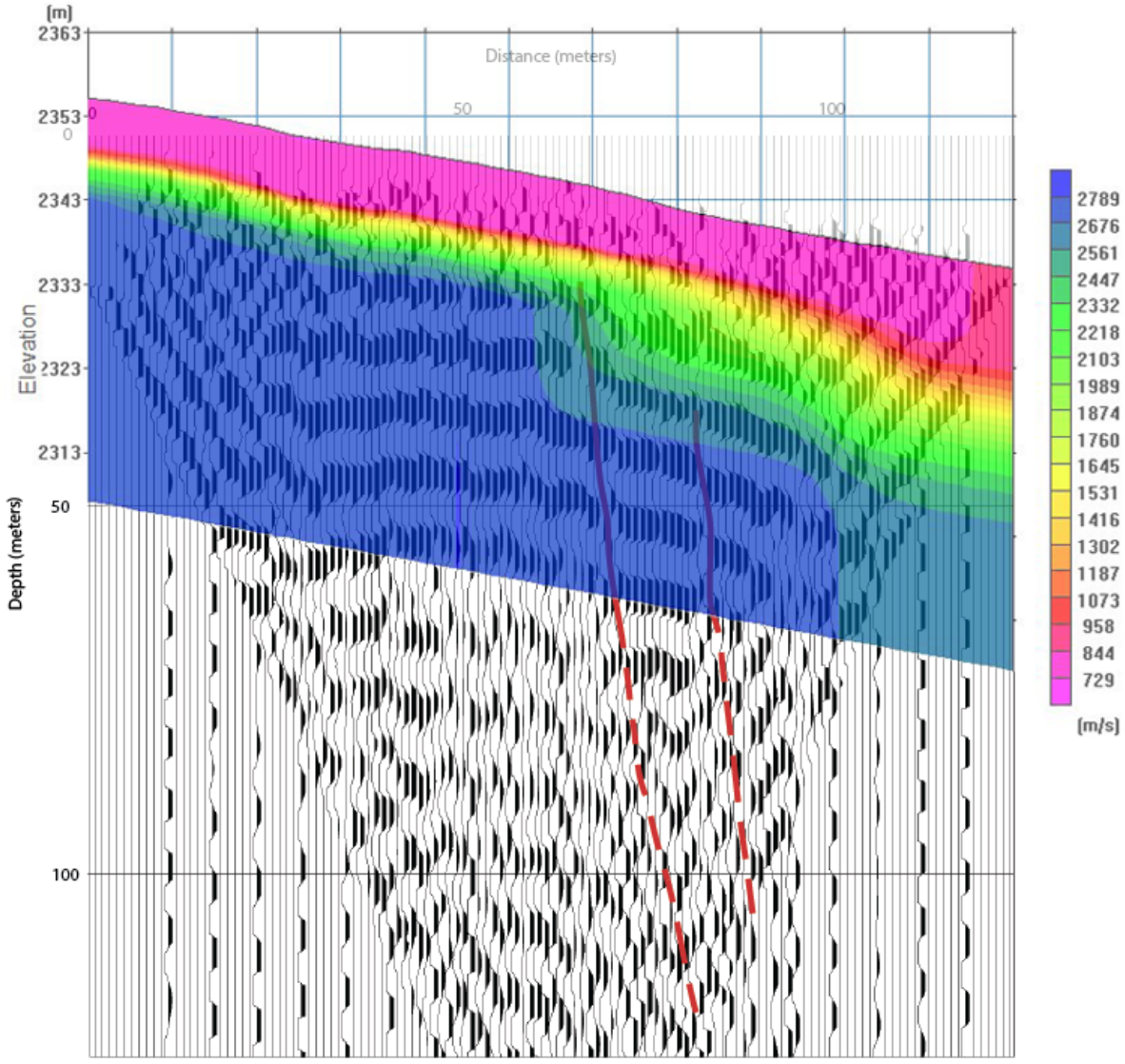

Figure 4.6 – Seismic refraction profile shown on top of seismic reflection profile scaled to the same size showing how the fault planes project with depth.

Chapter 5: Discussion and Conclusions

Late Quaternary deformation along the southern Granite Mountains was investigated with the goal of resolving kinematic and structural questions within the Laramide Orogeny and Wind River Basin as a whole. For the Ferris Mountains study area, fault scarp degradation modeling, seismic refraction, and seismic reflection imaging were used to examine the morphology and underlying structural geometry, respectively.

Photogrammetric surveys and fault scarp degradation modeling assessed the kinematic evolution of deformation. Calibration of the κ value from the known ages of corelated surfaces yielded a value of mass diffusivity for the region of 0.96 +/- 0.04. this value verry closely aligns with the value for the Lost River, Idaho values of 0.9 - 1 and thus it would be appropriate to apply that value given by Hanks (1984) and apply it in any future work. To calculate dip slip and extension rates via trigonometry, a range of dip angles is considered from 55 to 80 for the normal faults observed.

Seismic refraction and reflection imaging techniques assessed the geometry of the shallow subsurface structures. The shallow geophysical data collected at Cherry Creek supports the interpretation of a high - angle (83°) fault plane dipping to the north (Geomatrix Consultants inc., 1988). This aligns with historical beliefs unto the orientation of these faults across the region as well as in the adjacent Green and Seminoe mountain segments. Seismic profiling addressed whether there were several faults along the regolith benches and their relationships. Based on the refraction tomography the first fault exists near the 170-meter station while the second fault exists between the 192- and 202-meter stations. The velocity steps in these areas support the interpretation of two faults that are synthetic to each other where the fault further down slope is non- surface

rupturing. This fault placement is confirmed with the imaging from the reflection modeling an also identifies the high angle geometry where faults are dipping nearly vertically at 83°. The presence of a shallow granite bedrock unit as shown in the Geomatrix, (1988) trench logs is not supported from the refraction tomography. The seismic velocity within the first 10 meters depth is not nearly sufficient to support a shallow bedrock interpretation.

Geologic evidence for possible reverse faulting was only observed in one paleoseismic trench at Cherry Creek (Geomatix Consultants inc. 1988).However, shallow geophysics has now been documented to show extensional components of faulting which supports the historical belief that these are indeed normal faults (Almendinger, 1992; Love 1972). This indicates neotectonic activity in the northern Wind River Basin in the Owl Creek Mountains is not related to the extension in the Granite Mountains which is otherwise related to the continued collapse of the Sweetwater Graben.

Due to the perceived geometry of this fault being that of a listric normal fault, the dip slip rate becomes a valuable measurement for displacement of the upper portion of the fault, while the long-term extension rate predicts displacement at depth. Thus, long-term dip slip rates are estimated from 0.001 to 0.01 mm/yr at Cherry Creek (55-80°, respectively), 0.001 to 0.05 mm/yr at Pete Creek (55-80°, respectively), and 0.001 to 0.02 mm/yr at Arkansas Creek. In addition, the horizontal extension rate across the region is approximately 0.004 to 0.02 mm/yr at Arkansas Creek (55-80°, respectively), 0.002 to 0.03 mm/yr at Pete Creek (55-80°, respectively), and 0.002 to 0.03 mm/yr at Cherry Creek (55-80°, respectively). These values are not significantly different across the fault system and suggests a more uniform deformation rate.

Taking the estimated throw from the seismic refraction data of 10-13 meters and dividing it by the rate of uplift derived for the Q3 surface at Cherry Creek of 0.125 mm/yr an estimated age of fault initiation at this location is determined. This gives an estimated initiation date between 104 and 80 ka.

Implications for seismic hazards

The deformation in the Sough Granite Mountains is likely to continue given the granite mountains continue to sink from the crustal relaxation post Laramide orogeny. Fluid injection wells in the vicinity of this fault should be considered as well. Continued injection of wastewater can act as a lubricant for the fault planes at depth as well as reduce the effective stress within the region, therefore, with continued injection it would be expected that the faults remain active in the future. The proximity of the SGMFS to critical infrastructure outlined in the Geomatrix (1988) report is the reason this area is of interest for exploring the possibilities of seismic hazard. The maximum earthquake magnitude to potentially affect this region is 6.9 assuming the entire 18 km distance along the Ferris Mountains front were to rupture with more preferable estimates being at 6.6. Given the high degree of segmentation a smaller estimate of magnitude may be more likely. The dominant faulting mechanism here should be documented as normal faulting as these faults are not reactivated older Laramide structures as observed in the northern Wind River Basin (Gomez et. al, 2016).

Future Work

Although seismic imaging and photogrammetric methods where combined to produce a comprehensive model, future research would be beneficial to answer questions that arose from this study. An extension of the seismic reflection profile could be

considered in an attempt to identify the deeper structural trend, this however would only help to identify larger structural trends within the Sweetwater Graben and may prove non useful as the intended reflection survey yielded poor results. Increasing the length of the refraction profile would help to further the constrain on the geometry of synthetic fault splays in this location. Additional sUAV data could also provide more data from which more scarp profiles could be extracted to further estimate ages of units that have not been corelated to absolute ages previously.

References

Allmendinger, R.W. (1992). Fold and thrust tectonics of the Western United States exclusive of the accreted terranes: Geological Society of America, The Geology of North America v.G-3, p.583-607

Blackstone, D.L. (1991). Tectonic Relationships of the southeastern Wind River Range, Southwestern Sweetwater Uplift, and Rawlins Uplift, Wyoming: The Geological Survey of Wyoming, Report of Investigations no.47.

Blair, T. C. and McPherson, J. G. (2009). Processes and Forms of Alluvial Fans. Geomorphology of Desert Environments, pp. 413–467., doi:10.1007/978-1-4020-5719-9_14.

Case, J. C. and Green, J. A. (2000) Earthquakes in Wyoming: Wyoming State Geological Survey, Information Pamphlet, No. 6.

Fonstad, M. A., Dietrich, J. T., Courville, B. C., Jensen, J. L., & Carbonneau, P. E. (2013). Topographic Structure from Motion: a new development in photogrammetric measurement. Earth Surface Processes and Landforms, vol. 38, pp. 421–430., doi:10.1002/esp.3366.

Geomatrix Consultants inc. (1988). Seismotectonic evaluation of the northwestern Wind River Basin. Final Report prepared for the U.S. Bureau of Reclamation, Contract No. 6-CS-81-07310, p.116.

Gomez, F. (2016). Re-evaluation of late Quaternary deformation in the northern Wind River Basin, Wyoming, in: C. Grutzner & J. McCalpin (eds.), Proceedings of the 7th International INQUA Meeting on Paleoseismology, Active Tectonics, and Archeoseismology.

Hanks, T. C. (2000). The Age of Scarplike Landforms from Diffusion-Equation Analysis. Quaternary Geochronology; Methods and Applications. AGU Reference Shelf, American Geophysical Union (AGU), p. 313–338, doi:10.1029/rf004p0313.

Hanks, T. C., Bucknam, R. C., Lajoie, K. R., & Wallace, R. E. (1984). Modification of Wave-Cut and Faulting-Controlled Landforms. Journal of Geophysical Research: Solid Earth, v. 89, no. B7, pp. 5771–5790, doi:10.1029/JB089iB07p05771.

Jaworowski, C. (1988). Geomorphic Evidence for Neotectonism in Central Wyoming, U.S.A: Tectonophysics, v.163 (1989), p.333-337.

Keefer, W.R. (1965). Geologic History of Wind River Basin, Central Wyoming: Bulletin of the American Association of Petroleum Geologists, v.49, 1878-1892.

Keefer, W.R. (1970). Structural geology of the Wind River Basin, Wyoming: United States Geological Survey Professional Paper 495-D, 35 p.

Love, J.D. (1970). Cenozoic geology of the Granite Mountains area, central Wyoming: U. S. Geological Survey Professional Paper, C1-C154, P 0495-C.

Mattson, A., and Bruhn, R.L. (2001) Fault slip rates and initiation age based on diffusion equation modeling—Wasatch fault zone and eastern Great Basin: Journal of Geophysical Research, v. 106, no. B7, p. 13,739– 13,750., https://doi.org/10.1029/2001JB900003.

Mayer, Larry A. (1984). Dating Quaternary fault scarps formed in alluvium using morphologic parameters. Quaternary Research 22: 300-313.

Mears, B. Eckerle, W. P., Gilmer, D. R., Gubbels, T. L., Huckleberry, G. A., Marriott, H. J., ... & Yose, L. A. (1986). A Geologic tour of Wyoming from Laramie to

Lander, Jackson and Rock Springs: Geological Survey of Wyoming, Public Information Circular, no. 27.

Phillips, F. M., Zreda, M. G., Gosse, J. C., Klein, J., Evenson, E. B., Hall, R. D., ... & Sharma, P. (1997). Cosmogenic ^{36}Cl and ^{10}Be ages of Quaternary glacial and fluvial deposits of the Wind River Range, Wyoming. GSA Bulletin; November; v. 109; no. 11; p. 1453–1463.

Peterman, Z.E. and Hildreth R.A. (1978). Reconnaissance Geology and Geochronology of the Precambrian of the Granite Mountains, Wyoming: U.S. Geological Survey, Professional Paper 1055

Saleeby, J. (2003). Segmentation of the Laramide Slab—evidence from the southern Sierra Nevada region: Geological Society of America Bulletin, v.115, no. 6, p. 655-668.

Snoke, A.W. (1993). Geologic history of Wyoming within the tectonic framework of the North American Cordillera, in Snoke, A.W., J.R. Steidtmann, and S.M. Roberts, editors, Geology of Wyoming: Geological Survey of Wyoming Memoir No. 5, p. 2-56.

Wallace, R.E. (1977). Profiles and ages of young fault scarps, north-central Nevada. Geological Society of America Bulletin 88, 1,267–1,281.

Wang, X., Zhao, D., & Li, J. (2016) The 2013 Wyoming upper mantle earthquakes: Tomography and tectonic implications: Journal Geophysical Research: Solid Earth, 121, 6797–6808, doi:10.1002/ 2016JB013118.

Wells, D.L. and Coppersmith, K.J. (1984). New Empirical Relationships among Magnitude, Rupture Length, Rupture Width, Rupture Area, and Surface

Displacement: Bulletin of the Seismological Society of America, v. 36, p. 320–323, doi:10.1002/esp.2040.